

CHALMERS



Computational Modeling of Flow over a Spillway

In Vatnsfellsstífla Dam in Iceland

Master of Science Thesis

BJÖRN MARGEIRSSON

Department of Applied Mechanics

Division of Fluid Dynamics

CHALMERS UNIVERSITY OF TECHNOLOGY

Gothenburg, Sweden, 2007

Master's Thesis 2007:29

Master's Thesis 2007:29

Computational Modeling of Flow over a Spillway
In Vatnsfellsstífla Dam in Iceland

by

BJÖRN MARGEIRSSON

Department of Applied Mechanics,
CHALMERS UNIVERSITY OF TECHNOLOGY
Göteborg, Sweden, 2007

Computational Modeling of Flow over a Spillway

In Vatnsfellsstífla Dam in Iceland

BJÖRN MARGEIRSSON

© BJÖRN MARGEIRSSON, 2007

Master's Thesis 2007:29

ISSN 1652-8557

Department of Applied Mechanics
Chalmers University of Technology
SE-412 96 Göteborg
Sweden
Telephone +46 (0)31 772 1000

Abstract

The main dam of the hydroelectric scheme in Vatnsfell, Iceland, is 30 m high, filled with rock and is equipped with a concrete slab facing. Two spillways (an overfall spillway and a bottom outlet) are adopted for flood release and share a common energy dissipating stilling basin. In this work the flow over the overfall spillway and in the stilling basin is modeled with the CFD-software FLUENT. The aspects that are evaluated and investigated include the discharge capacity of the spillway and the water pressure on it, the forces on the baffles in the stilling basin and the velocity profile for the water flow out of the basin. The results are validated by comparison with results from hydraulic model studies on the subject.

A quite good agreement is achieved for the discharge capacity of the spillway and the pressure acting on it. The same can be said about the velocity profile at the downstream end of the stilling basin. On the other hand, worse agreement for other properties of the flow implies that more work and/or computational power are needed in order to improve the grid resolution and thereby better resolve the flow.

Keywords: *CFD, FLUENT, VOF, 3D flow, spillway, discharge capacity, stilling basin*

Preface

This work aims at computationally modeling water flow over a spillway which is a part of the Vatnsfell hydroelectric power plant in Iceland. In 1999 hydraulic model studies were done for the Vatnsfell dam by Vattenfall in Sweden. Vattenfall not only investigated the flow over the spillway but also the flow through a bottom outlet and a common spatial stilling basin. The present study includes the same geometry as in the hydraulic model study except the bottom outlet is excluded and only a small emphasis is placed on the stilling basin. The work is thus focused on the flow in the spillway.

An introduction to the hydraulic concerns at Vatnsfell is presented in chapter 1 along with the software used and experimental data. Chapter 2 is an introduction to the governing equations of fluid motion, turbulence modeling and to the discharge capacity of spillways. Chapter 3 discusses the numerical aspects of the computations. The computational results are introduced and discussed in chapter 4. The main conclusions can be found in chapter 5 and also some ideas of future work. Finally, appendix A shows the layout of the subject and appendix B is basically a tutorial for the VOF method in FLUENT.

Acknowledgements

I would like to express my gratitude to the financial sponsors of this project; Landsvirkjun (Iceland National Power Company) and Almenna Consulting Engineers. My special thanks go to my mentor at Almenna Consulting Engineers, Ólafur Árnason, for his support and practical guidance during the work.

I would also like to thank my supervisor, Dr. Håkan Nilsson, for his very valuable guidance, especially theoretical and practical suggestions concerning the calculations but also when writing this report. The most of the work was carried out in Iceland but that didn't prevent Håkan from assisting me with his numerous and precious e-mails.

Last but not least, I would like to thank my loving wife, Rakel Ingólfssdóttir, for endless patience and tolerance.

Nomenclature

Roman Symbols

a	Speed of sound [m/s]
B	Spillway crest length [m]
C	Discharge coefficient [$\text{m}^{1/2}\text{s}^{-1}$]
$C_{\epsilon 1}, C_{\epsilon 2}, C_{\mu}$	Constants in the standard k- ϵ model of turbulence [-]
d_{50}	Median diameter [m]
\vec{F}	External body force [N]
g_i	Gravity tensor [m/s^2]
G_b	Generation of turbulence kinetic energy due to buoyancy [$\text{kg}/\text{m}/\text{s}^3$]
G_k	Generation of turbulence kinetic energy due to the mean velocity gradients [$\text{kg}/\text{m}/\text{s}^3$]
H	Head [m]
k	Turbulent kinetic energy [m^2/s^2]
\dot{m}	Mass flow rate [kg/s]
M_t	Turbulent Mach number [-]
p	Pressure [Pa]
Pr_t	Turbulent Prandtl number for energy [-]
Q	Flow discharge [m^3/s]
R	Gas constant for air [J/kg/K]
S_k	Source term [$\text{kg}/\text{m}/\text{s}^3$]
S_{ϵ}	Source term [$\text{kg}/\text{m}/\text{s}^4$]
\mathbf{u}, u_i	Velocity vector/tensor [m/s]
$\overline{u_i}$	Mean components of velocity tensor [m/s]
u'_i	Fluctuating components of velocity tensor [m/s]
T	Temperature [K]
Y_M	Fluctuating dilation in compressible turbulence [$\text{kg}/\text{m}/\text{s}^3$]

Greek Symbols

α	Volume fraction [-]
β	Coefficient of thermal expansion [1/K]
γ	Adiabatic index (isentropic expansion factor) for air [-]
ε	Turbulent dissipation [m^2/s^3]
μ	Dynamic viscosity [kg/m/s]
μ_t	Turbulent eddy viscosity [kg/m/s]
ν	Kinematic viscosity [m^2/s]
ρ	Density [kg/m^3]
σ_k	Turbulent Prandtl number for k [-]
σ_ε	Turbulent Prandtl number for ε [-]
$\partial_0 u_i$	Time derivative of velocity tensor [m/s^2]
$\partial_j u_i$	Partial j-derivative of velocity tensor [$1/\text{s}^2$]

Super- and Subscripts

<i>exp, EXP</i>	Experimental
<i>CFD</i>	Calculated; Computational Fluid Dynamics
<i>p</i>	Pressure [Pa]
<i>RANS</i>	Reynolds-averaged Navier-Stokes equations
<i>t</i>	Turbulent

Contents

Abstract.....	i
Preface.....	v
Acknowledgements.....	vi
Nomenclature.....	vii
Roman Symbols.....	vii
Greek Symbols.....	viii
Super- and Subscripts.....	viii
Contents.....	ix
1 Introduction.....	1
1.1 Hydraulic Concerns at Vatnsfell.....	1
1.2 Software.....	2
1.3 Limitations.....	3
1.4 Experimental Data.....	3
2 Theory.....	4
2.1 Equations of Motion.....	4
2.2 Turbulence Model.....	4
2.3 Volume of Fluid (VOF) Model in FLUENT.....	6
2.4 Discharge Capacity of Spillways.....	8
3 Numerical Aspects.....	9
3.1 Solver.....	9
3.2 Computational Domain.....	9
3.3 Cases.....	10
3.4 Boundary Conditions.....	11
3.5 Grids.....	11
4 Results and Discussion.....	18
4.1 Discharge Capacity.....	18
4.2 Water Surface Profile along Side Walls.....	19
4.3 Pressure on Spillway Chute.....	20
4.4 Basin Side-Wall Height.....	23
4.5 Forces on Baffle Blocks.....	25
4.6 Pressure Acting on End Sill.....	26
4.7 Velocity Profile at End Sill.....	27
5 Conclusions and Future Work.....	29
References.....	30
Appendix A Layout of Vatnsfell Spillway and Connected Structure	
Appendix B How to Get a Well Resolved Surface with the VOF Method in FLUENT	

1 Introduction

1.1 Hydraulic Concerns at Vatnsfell

The overfall spillway at Vatnsfell (see Figure 1) is an example of a converging overfall spillway or chute spillway. The main purpose of it is to keep down accidental flooding situations and function thereby as an emergency spillway. It is situated on top of the main dam in Vatnsfell and consists mainly of three parts; an overfall crest, a funnel and a chute (see layout in Appendix A).



Figure 1. The converging overfall spillway at Vatnsfell during flood discharge

Cost optimization with regard to the elevation of the parapet wall, intake to the power house and saddle dams determines the shape and orientation of the spillway crest. The crest elevation of +563.5 m and crest length of 50.0 m should result in a discharge capacity of approximately $280 \text{ m}^3/\text{s}$ if calculated with a common correlation (see Chapter 2.4). The crest is curved so that the chute can more easily converge to a width of 10.0 m. The curvature of the crest can be noticed in Figure 2.



Figure 2. The curved spillway crest as seen from above

Governing factors in the design of the chute are of economical nature along with the existence of a bridge structure over the chute. In order to use the load-bearing capacity of the retaining walls of the dam fill and chute slab the spillway is placed deep in the dam fill.

The stilling basin is an energy dissipation structure. As the water flows down the basin it is impacted by increasing channel width by a decrease in the required tail water depth to achieve a reduction in the length of a hydraulic jump. A maximum flow velocity is defined as 5.0 m/s where the water exits the basin and therefore a number of baffles are spread over the basin. The size and position of the baffles are actually not only determined by the flow over the spillway but also by the flow through the bottom outlet. Downstream the stilling basin a 35 m long section of rock rip-rap is laid down to protect the river bed. The protected area has an adverse slope so that its downstream end is about 1 m higher than its upstream end.

The main purpose of this work is to numerically determine the water surface height in the spillway. This is done for a few cases of different discharge and compared to experimental data. The flow depth along the transitional walls, the forces acting on the chute slab, and the flow in the stilling basin are also investigated.

1.2 Software

The 3D-geometry was drawn in the CAD program Autodesk INVENTOR. The convenient feature of importing CAD-geometries was utilized in the grid generation program GAMBIT before designing the grids. FLUENT was the CFD solver used and it was also used for post-processing along with MATLAB. Other well known CFD codes that have been used in this area are FLOW-3D and STAR-CD. The VOF method in FLUENT is used to locate the interface between water and air (see Appendix B).

1.3 Limitations

The calculations were mostly done on a single portable computer and a single desktop computer which must be considered an extremely limited computational resource for such a complicated CFD-project. The high Reynolds number and the requirements for the resolution of the water surface together yield a need for a very large computational grid.

Because of the limited computational resources and the limited time for the project only the spillway was investigated but not the bottom outlet. Although the stilling basin is included in the geometry and in the calculations, not much effort is put in refining the grid in the basin. This is done to spare computational power and because the VOF method would anyhow have difficulties in locating the hardly definable water surface there.

1.4 Experimental Data

The experimental data used for comparison was provided in the report Vatnsfell Hydropower Project, Iceland – Hydraulic Model Studies of Flood Discharge Structures [4]. These experimental results were used when the hydroelectric scheme was designed for Landsvirkjun. The main idea behind the present study was to examine if and how accurately the flow in the spillway and the stilling basin could be computationally modeled.

The experiments include measurements for the discharge capacity of the spillway, flow depth along its transitional walls and forces acting on the chute slab. All of these measurements were used for validation of the CFD-modeling. The same is true for the measurements that were done for the water height along the left side-wall of the basin, pressure on the end sill and the flow velocity above the end sill. On the other hand, only some of the baffle blocks pressure measurements were used for validation. Flow velocity downstream the rip-rap was tested in the experiments but not investigated in the present study.

Some other aspects were tested in the experiments but not used for validation, e.g. discharge capacity of the bottom outlet, swirling flow at the bottom intake, and risk for sedimentation.

2 Theory

2.1 Equations of Motion

A flow is incompressible when changes in density are negligible, both with respect to time and space. The continuity equation for compressible flow:

$$\partial_0 \rho + \partial_i (\rho u_i) = 0 \quad (1)$$

which can be derived from the principle of mass conservation can thus be simplified for incompressible flow to

$$\partial_i u_i = 0 \quad (2)$$

In a similar way the compressible momentum equations can be derived from the principle of momentum conservation and simplified to the incompressible momentum equations:

$$D_0 u_i = -\frac{1}{\rho} \partial_i p + \nu \partial_j \partial_j u_i \quad (3)$$

where D_0 is the substantial or material derivative defined as

$$D_0 \equiv \partial_0 + u_j \partial_j \quad (4)$$

The continuity equation, the momentum equations, and an energy equation (which is not presented here) are usually referred to as the Navier-Stokes equations. For further details, see [2].

2.2 Turbulence Model

One of the main characteristics of turbulent flow is fluctuating velocity fields. These fluctuations cause mixing of transported quantities like momentum, energy and species concentration and thereby also fluctuations in the transported quantities. Because of the small scales and high frequencies of the fluctuations they are too computationally expensive to simulate directly in practical engineering situations. Instead, the instantaneous governing equations are time-averaged to remove the small scales and the result is a set of less expensive equations containing additional unknown variables. These unknown (turbulence) variables are determined in terms of modeled variables in turbulence models.

This process of time-averaging is called Reynolds averaging. When this is done the solution variables in the instantaneous Navier-Stokes equations are decomposed into the mean (time-averaged) and fluctuation components (Reynolds decomposition). For the velocity components:

$$u_i \equiv \bar{u}_i + u_i' \quad (5)$$

where \bar{u}_i and u_i' are the mean and fluctuating velocity components respectively. Scalar variables are decomposed in a similar way. When expressions of this form for the flow variables are substituted into the instantaneous continuity and momentum equations and a

time (ensemble) average is taken the Reynolds-averaged Navier-Stokes (RANS) equations are yielded. They can be written as

$$\frac{\partial \rho}{\partial t} + \frac{\partial}{\partial x_i}(\rho u_i) = 0 \quad (6)$$

$$\frac{\partial}{\partial t}(\rho u_i) + \frac{\partial}{\partial x_j}(\rho u_i u_j) = -\frac{\partial p}{\partial x_i} + \frac{\partial}{\partial x_j} \left[\mu \left(\frac{\partial u_i}{\partial x_j} + \frac{\partial u_j}{\partial x_i} - \frac{2}{3} \delta_{ij} \frac{\partial u_l}{\partial x_l} \right) \right] + \frac{\partial}{\partial x_j} \left(-\overline{\rho u_i' u_j'} \right) \quad (7)$$

Here the overbar on the mean velocity has been dropped. The velocities and other solution variables now represent time-averaged values instead of instantaneous values. The additional terms that have appeared ($-\overline{\rho u_i' u_j'}$) are called Reynolds stresses and must be modeled in order to close equation (7).

The turbulence model that is used in the present study is the standard k- ϵ model. It is one of the two-equation models which are considered the simplest of the so called complete models of turbulence. Ever since it was proposed in 1972 its popularity in industrial flow simulations has been explained by its robustness, economy and reasonable accuracy for a wide range of turbulent flows. The model is a semi-empirical model based on modeled transport equations for the turbulence kinetic energy (k) and its dissipation rate (ϵ).

The turbulence kinetic energy, k, and its rate of dissipation, ϵ , are obtained from the following transport equations:

$$\frac{\partial}{\partial t}(\rho k) + \frac{\partial}{\partial x_i}(\rho k u_i) = \frac{\partial}{\partial x_j} \left[\left(\mu + \frac{\mu_t}{\sigma_k} \right) \frac{\partial k}{\partial x_j} \right] + G_k + G_b - \rho \epsilon - Y_M + S_k \quad (8)$$

and

$$\frac{\partial}{\partial t}(\rho \epsilon) + \frac{\partial}{\partial x_i}(\rho \epsilon u_i) = \frac{\partial}{\partial x_j} \left[\left(\mu + \frac{\mu_t}{\sigma_\epsilon} \right) \frac{\partial \epsilon}{\partial x_j} \right] + C_{1\epsilon} \frac{\epsilon}{k} (G_k + C_{3\epsilon} G_b) - C_{2\epsilon} \rho \frac{\epsilon^2}{k} + S_\epsilon \quad (9)$$

G_k represents the generation of turbulence kinetic energy due to the mean velocity gradients:

$$G_k = -\overline{\rho u_i' u_j'} \frac{\partial u_j}{\partial x_i} \quad (10)$$

G_b is the generation of turbulence kinetic energy due to buoyancy:

$$G_b = \beta g_i \frac{\mu_t}{Pr_t} \frac{\partial T}{\partial x_i} \quad (11)$$

where g_i is the component of the gravitational vector in the i-th direction and $Pr_t = 0.85$ is the turbulent Prandtl number for energy. β is the coefficient of thermal expansion and defined as

$$\beta = -\frac{1}{\rho} \left(\frac{\partial \rho}{\partial T} \right)_p \quad (12)$$

Y_M represents the contribution of the fluctuating dilatation in compressible turbulence to the overall dissipation rate:

$$Y_M = 2\rho\varepsilon M_t^2 \quad (13)$$

where M_t is the turbulent Mach number, defined as

$$M_t = \sqrt{\frac{k}{a^2}} \quad (14)$$

where a is the speed of sound:

$$a = \sqrt{\gamma RT} \quad (15)$$

The approach used in the standard k- ε model to model the Reynolds stresses is the Boussinesq approach. The Boussinesq assumption relates the Reynolds stresses to the mean velocity gradients:

$$-\overline{\rho u_i' u_j'} = \mu_t \left(\frac{\partial u_i}{\partial x_j} + \frac{\partial u_j}{\partial x_i} \right) - \frac{2}{3} \left(\rho k + \mu_t \frac{\partial u_i}{\partial x_i} \right) \delta_{ij} \quad (16)$$

where the turbulent eddy viscosity is a function of k and ε :

$$\mu_t = \rho C_\mu \frac{k^2}{\varepsilon} \quad (17)$$

$C_{\varepsilon 1}$, $C_{\varepsilon 2}$ and C_μ are constants having the following values respectively: 1.44, 1.92, 0.09. σ_k and σ_ε are the turbulent Prandtl numbers for k and ε and have the following values respectively: 1.0 and 1.3. S_k and S_ε and are user-defined source terms. For further details of turbulence modeling, see [1].

The choice of turbulence model is probably not very important for the solution in this study. On the other hand, resolving the surface between the water and air, resolving the turbulent boundary layers close to walls, and defining the boundary conditions has a great influence on the solution. Because of that no effort was put in trying other turbulence models than the standard k- ε model.

2.3 Volume of Fluid (VOF) Model in FLUENT

The VOF method is based on the assumption that the two fluids are not interpenetrating. Each phase (fluid) is given a variable that accounts for how much percentage of each computational cell is occupied by the phase. This variable is called a volume fraction of the phase. The volume fractions of all phases sum up to unity in each computational cell. The fields for all variables and properties are shared by the phases and represent volume-averaged values. Variables and properties represent either only one phase or a mixture of phases in a given cell depending on the volume fractions of the phases in the cell. Denoting α_q as the volume fraction of the q -th phase three possibilities for a given cell can be noted:

- i) $\alpha_q = 0$: the cell is empty of the q-th phase,
- ii) $\alpha_q = 1$: the cell is full of the q-th phase,
- iii) $0 < \alpha_q < 1$: the cell contains the interphase between the q-th phase and one or more phases.

The presence of the component phases in each cell determines the properties appearing in the transport equations. In a system with n phases the property p in each cell is given by

$$p = \sum_{q=1}^n \alpha_q p_q \quad (18)$$

The momentum equation is solved throughout the domain, and the phases share the resulting velocity field. The momentum equation, stated below in a slightly different way from before, is dependent on the volume fractions of all phases through the properties ρ and μ :

$$\frac{\partial}{\partial t}(\rho \bar{u}) + \nabla \cdot (\rho \bar{u} \bar{u}) = -\nabla p + \nabla \cdot \left[\mu (\nabla \bar{u} + \nabla \bar{u}^T) \right] + \rho \bar{g} + \bar{F} \quad (19)$$

Here ρ is the density, μ is the dynamic viscosity, p is the static pressure and finally $\rho \bar{g}$ and \bar{F} are the gravitational body force and external body forces respectively.

For the turbulence a single set of the turbulence transport equations (5) and (6) are solved and turbulence variables (i.e. k and ε) are shared by phases throughout the whole field. To be able to determine precisely the water surface it is significant to have a sudden transition for the volume fraction between 0 and 1. Therefore it should be noted that it is important to use a discretization scheme that minimizes the numerical diffusion (numerical discretization error) where the volume fraction suddenly changes its value.

2.4 Discharge Capacity of Spillways

According to [4] the flow discharge through an overfall spillway can be expressed by

$$Q = CBH^{\frac{3}{2}} \quad (20)$$

where Q denotes the flow discharge, C discharge coefficient, B the spillway crest length and H head measured from the crest to the unaffected upstream water stage. The value of the discharge coefficient normally doesn't vary much from 2.2.

3 Numerical Aspects

In this chapter some numerical considerations are discussed. The solver and the computational domain are described and the different cases defined. The setup of boundary conditions is presented and finally some basic information about the grids.

3.1 Solver

The segregated solver is used with the PISO pressure-velocity coupling scheme. Since the second order discretization for momentum resulted in an unstable solution the first order scheme was used. For the VOF-method the PRESTO! scheme is preferable as the pressure interpolation scheme and also the modified HRIC scheme for the volume fraction equations in order to improve the sharpness of the interface between the two faces. Turbulence is not emphasized and therefore only first order scheme is used when solving for it. The grids are hexagonal and aligned with the flow in the biggest part of the domain and thus should a first order scheme in general give reasonable accuracy.

Notable is the fact that using under-relaxation factors as low as 0.01 – 0.1 was necessary in order to achieve convergence when performing some of the calculations. These values are even lower than the recommended ones, see [1].

3.2 Computational Domain

The flow over the spillway is 3D and even though some symmetry can be found in the spillway itself the stilling basin is not symmetric. Therefore it was decided to model the flow in 3D. Since the main goal was not to locate the water surface in the stilling basin, the end sill of the stilling basin was set as the downstream end of the computational domain in most of the cases (see chapter 3.3). In order to better resolve the flow in the basin some additional volume was added downstream the basin for one single case so that the rock rip-rap was included. For most cases the baffles in the basin were included in the geometry and that along with a large forebay reservoir resulted in a fairly big and complicated computational domain. The way the spillway chute converges to a constant width of 10.0 m also puts into the complexity. However, the longitudinal curvature of the spillway crest was excluded which made meshing of the reservoir easier (see Figure 3 and Figure 4). Yet another simplification in the geometry can be found in the chute cover and splitter wall.

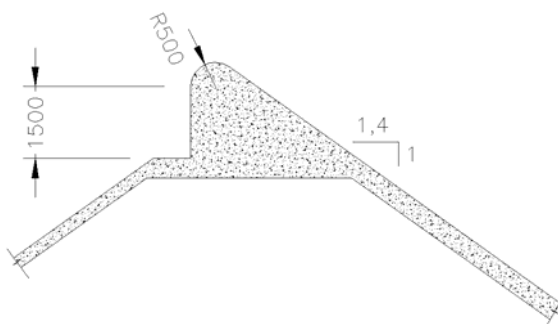


Figure 3. Crest of the converging spillway – longitudinal profile

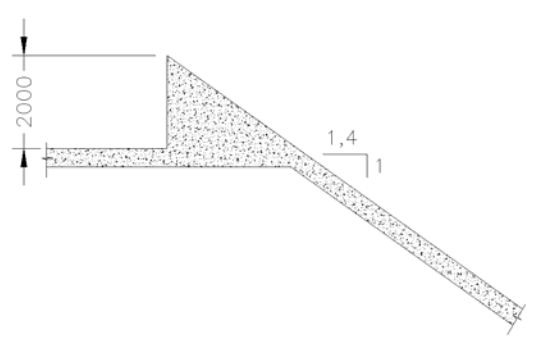


Figure 4. Simplified crest of the converging spillway – longitudinal profile

The reservoir reaches out 80 m upstream from the spillway crest and is approximately 175 m wide. This is done to secure stable flow rates and that the unaffected water level that

is used to calculate the discharge capacity (see equation 20) is reached. Figure 5 shows the computational domain from above as a whole.

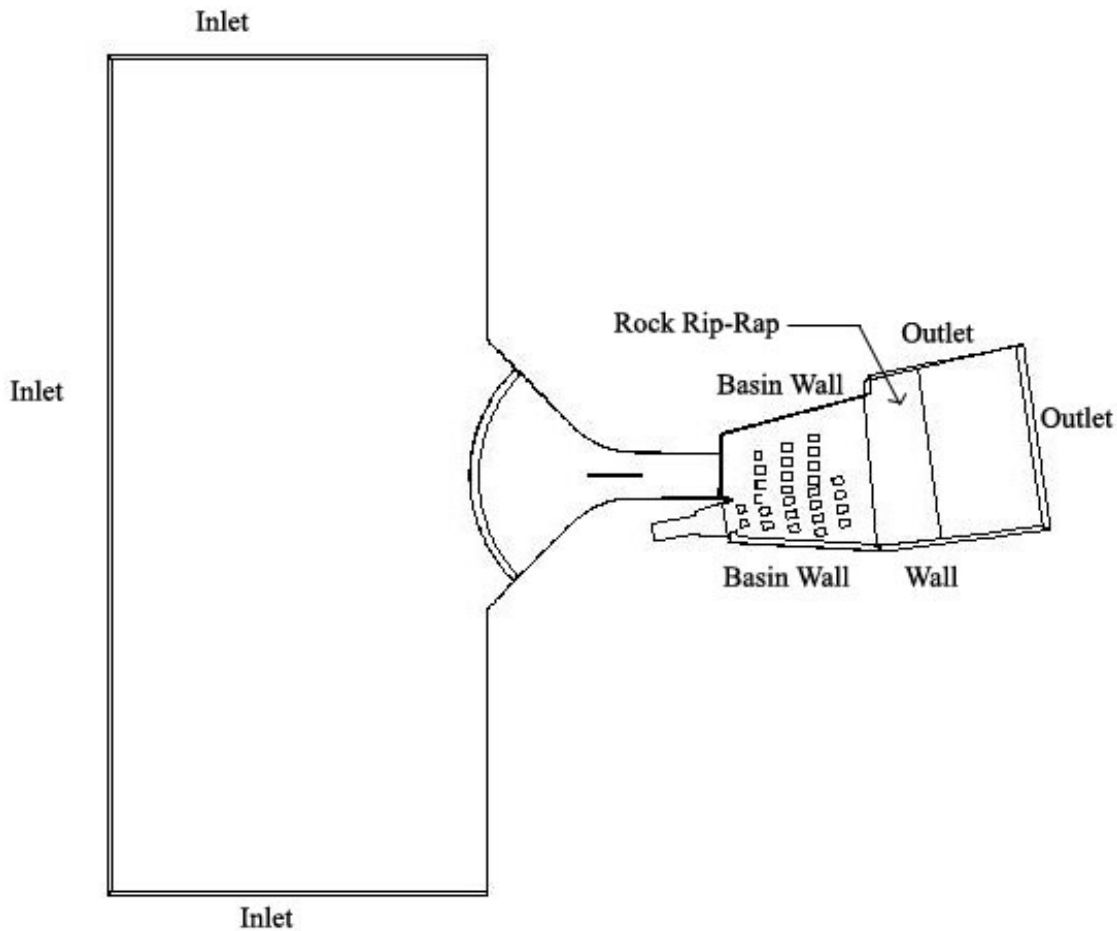


Figure 5. The computational domain as seen from above

3.3 Cases

Nine different steady flow cases were studied with flow discharge ranging from 50 m³/s to 350 m³/s (see Table 1). All of the cases studied included the stilling basin except nr. 8 which concentrated on the spillway. By excluding the basin and decreasing the forebay reservoir it became possible to better resolve the flow in the spillway itself instead of spending computational power in the basin and reservoir too.

Table 1. Cases

Case nr.	Discharge (m ³ /s)	Domain size	Case results in chapter
1	50	Full but rip-rap excluded	4.1
2	100	Full but rip-rap excluded	4.1
3	150	Full but rip-rap excluded	4.1
4	200	Full but rip-rap excluded	4.1
5	250	Full but rip-rap excluded	4.1
6	300	Full but rip-rap excluded	4.1, 4.2, 4.5
7	350	Full but rip-rap excluded	4.1
8	300	Only spillway and a smaller reservoir	4.2 - 4.3
9	300	Full	4.4 - 4.7

3.4 Boundary Conditions

A mass inflow boundary condition was used for the back and both sides of the reservoir. Defining turbulence intensity and hydraulic diameter was the chosen turbulence specification method for the inflow boundaries. Turbulence intensity was defined as 5 % and hydraulic diameter as 160 m for the left and right inlets of the reservoir and 320 m for the inlet at the back of the reservoir. The values for hydraulic diameter were decreased according to the decrease in reservoir size in case 8. At the walls the common non-porous and no-slip boundary condition was used;

$$u_i = 0 \quad (21)$$

A roughness of 5 mm was defined for all walls, where wall-functions were used. The outlet of the domain was defined as a pressure outlet with the static gauge pressure of 0 Pa, backflow turbulence intensity of 10 % and backflow hydraulic diameter of 60 m. A pressure outlet boundary condition was also used for faces above the domain with the static gauge pressure of 0 Pa, backflow turbulence intensity of 5 % and the backflow hydraulic diameter defined as the circumference of the face representing the outlet.

3.5 Grids

The grids are built up of hexagonal cells as much as possible and an overview of the grid for case 8 is presented in Figure 6. The forebay reservoir is meshed completely with hexagonal cells. Because of too high skewness in hex-mesh in the upper part of the spillway chute some part of it was meshed with hex-wedge-mesh (see Figure 7), which is not of as high quality as the hex-mesh. On the other hand, the rest of the spillway chute is completely hex-meshed (see Figure 8 and Figure 9).

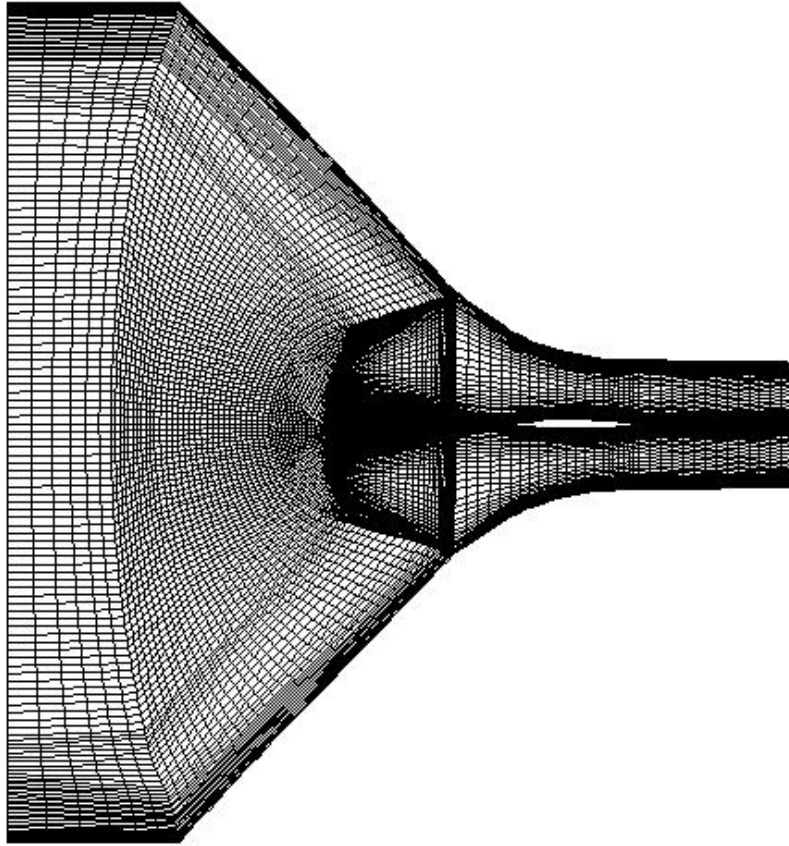


Figure 6. Overview of the grid for case 8

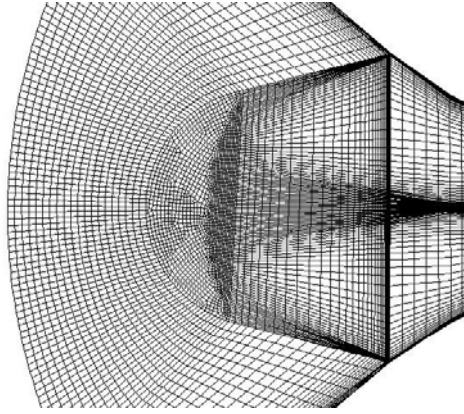


Figure 7. Mesh of the spillway bottom, showing the hex-wedge elements in the upper part of the spillway chute. Case 8

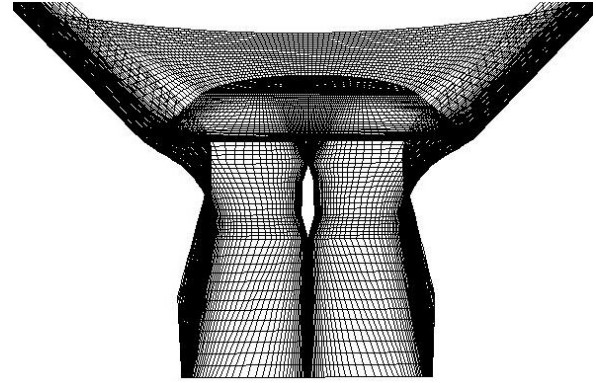


Figure 8. The mesh of the spillway chute bottom and sidewalls looking upstream. Case 8

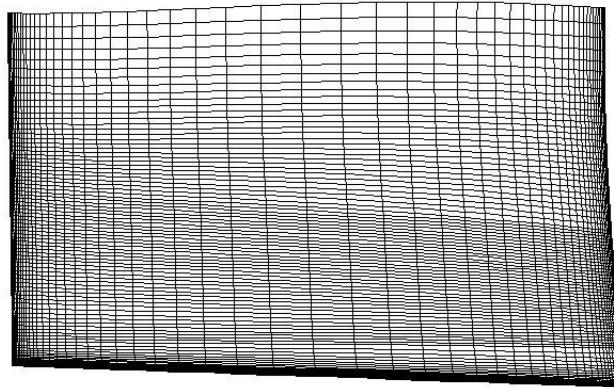


Figure 9. Cut through the hex-mesh in half of the spillway chute looking upstream. The cut is made perpendicular to the middle of the splitter wall and shows how much finer the mesh is close to the splitter wall to the left, the spillway chute wall to the right and the chute bottom. Case 8

In order to resolve the turbulent boundary layers the hex-mesh is made a lot finer close to the walls and the bottom of the spillway chute. This results in a rather fine and computationally expensive mesh of 1,392,594 cells. Figure 9 shows a cut through the mesh to visualize the near-wall refinement.

In case 9 the preferable hex-mesh was also used as much as possible. An overview of the mesh is presented in Figure 10. In this case the upper part of the stilling basin is hex-meshed (see Figure 12) but because of the energy dissipating baffles spread out in the basin bottom it was necessary to use tetrahedral cells in most of the lower part of the basin (see Figure 11). Tet-mesh is both a lot more expensive in terms of computational power (craves more cells and thereby more calculations) and also doesn't give as accurate results as the hex-mesh. However, since the flow is not well resolved in the upper part of the domain compared to the other cases, the mesh sparingly consisted of 497,664 computational cells.

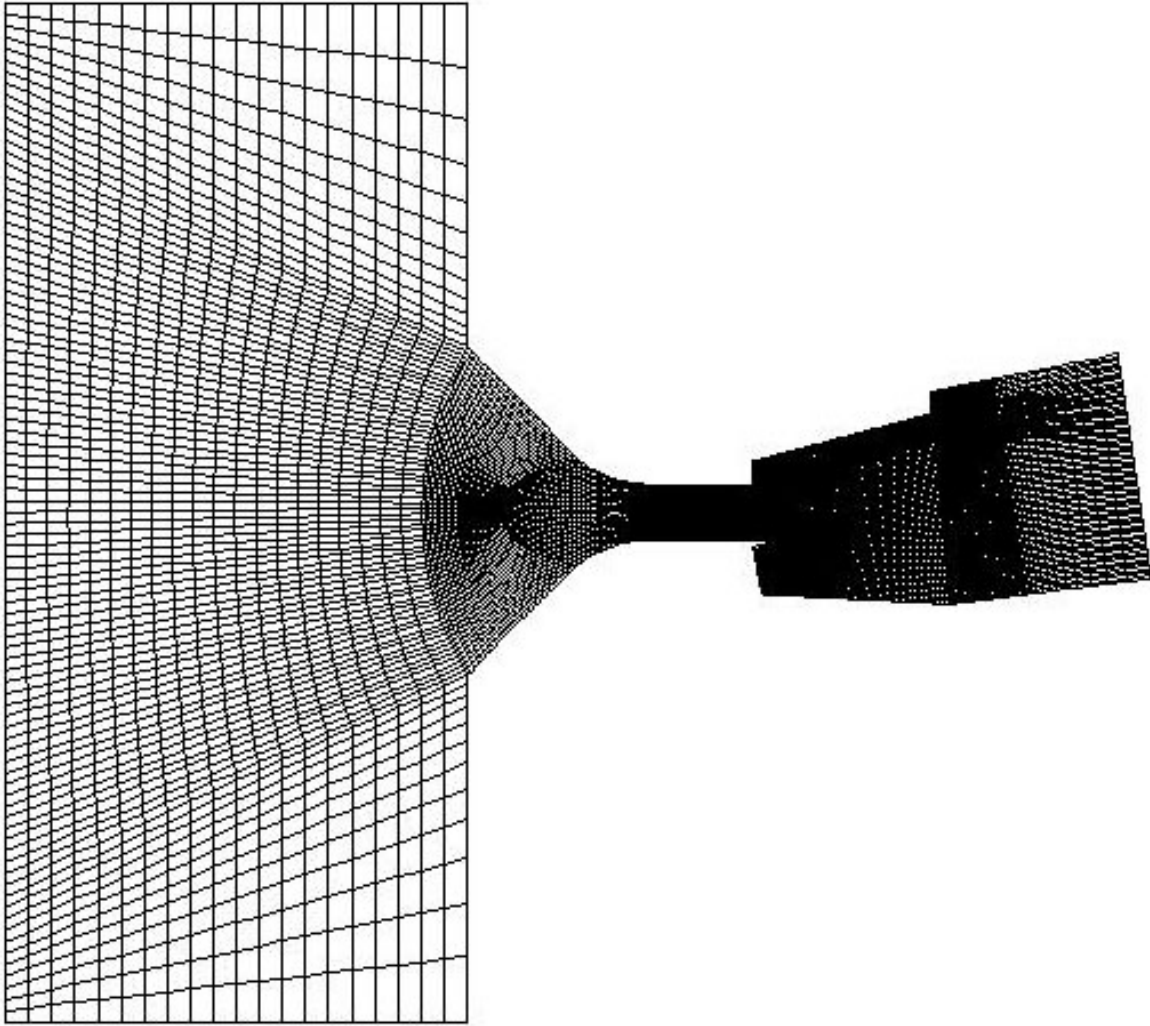


Figure 10. Overview of the grid in case 9

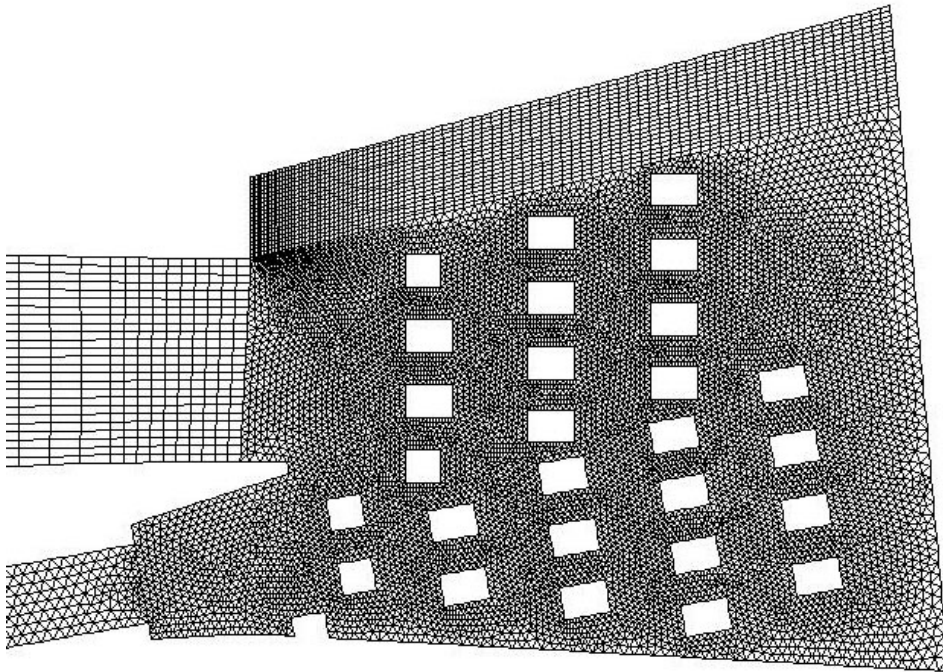


Figure 11. Mesh of the basin bottom and the downstream end of spillway chute. The existence of baffles makes a hex-mesh difficult to use in most of the basin bottom. Case 9

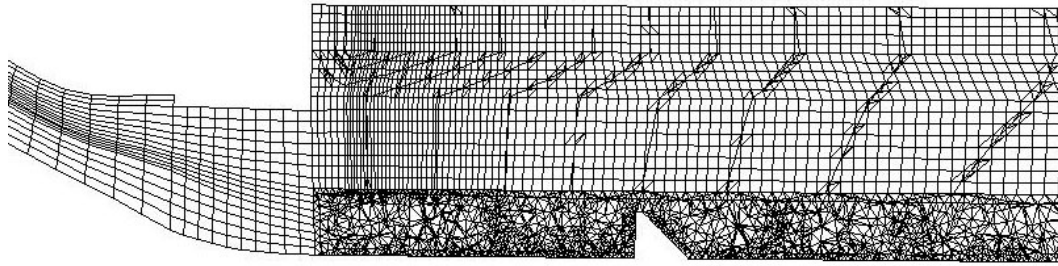


Figure 12. Cut through the mixed mesh in the stilling basin and the downstream end of the hex-meshed spillway chute. The cut is made in the middle of the spillway chute. Case 9

The rock rip-rap downstream the stilling basin was not precisely modeled. A few irregular canals were made perpendicular to the water flow downstream the basin as can be seen in Figure 13. The depth of these canals is around 1 m and they represent the upper section of rip-rap with median diameter $d_{50} \geq 1200$ mm. Downstream this approximately 10 m long section is a bigger section of rip-rap with median diameter $d_{50} \geq 400$ mm (see [3], p. 7) but this is only modeled in the present study as a wall with the same roughness as other walls.

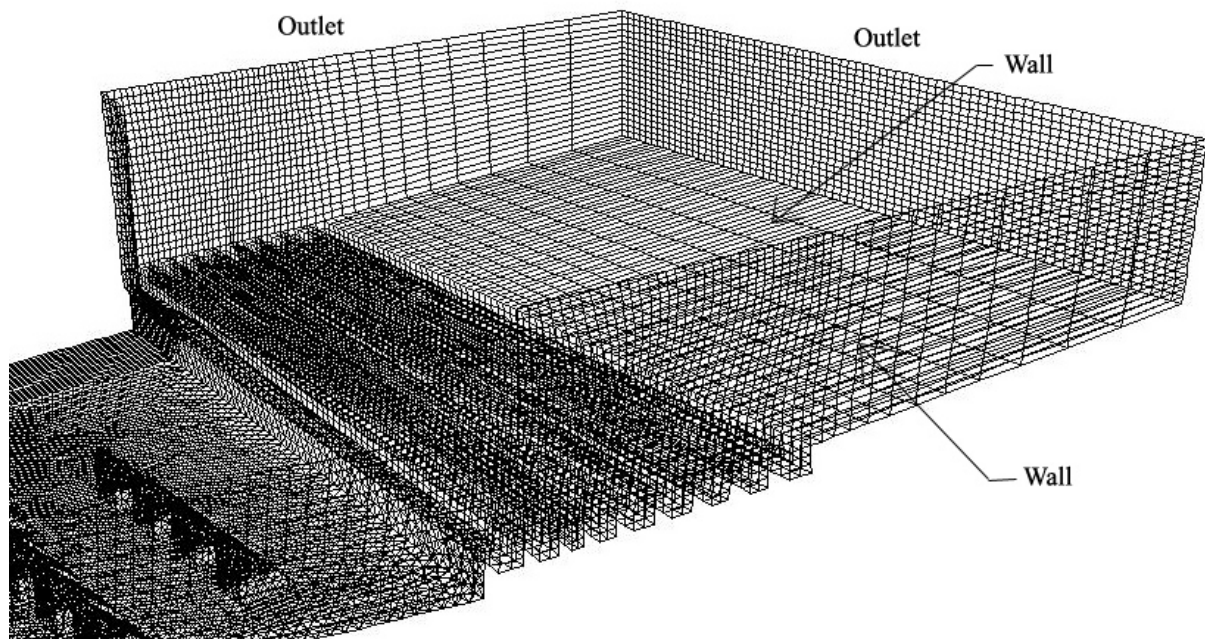


Figure 13. Mesh of the rock rip-rap and the downstream end of the stilling basin bottom also showing the surrounding walls and outlets to the left and downstream. Case 9

In cases 1-7, the rock rip-rap downstream the stilling basin is excluded and only a very rough tet-mesh is used in the whole stilling basin. On the other hand, the forebay reservoir is meshed with much finer hex-mesh than in case 9. The reason is that the purpose of cases 1-7 was only to study the flow discharge and its relation to the reservoir water level. Still, case 6 was also used to calculate the forces on two baffle blocks and the results compared to the results from case 9. An overview of the grid used in case 1 can be seen in Figure 14.

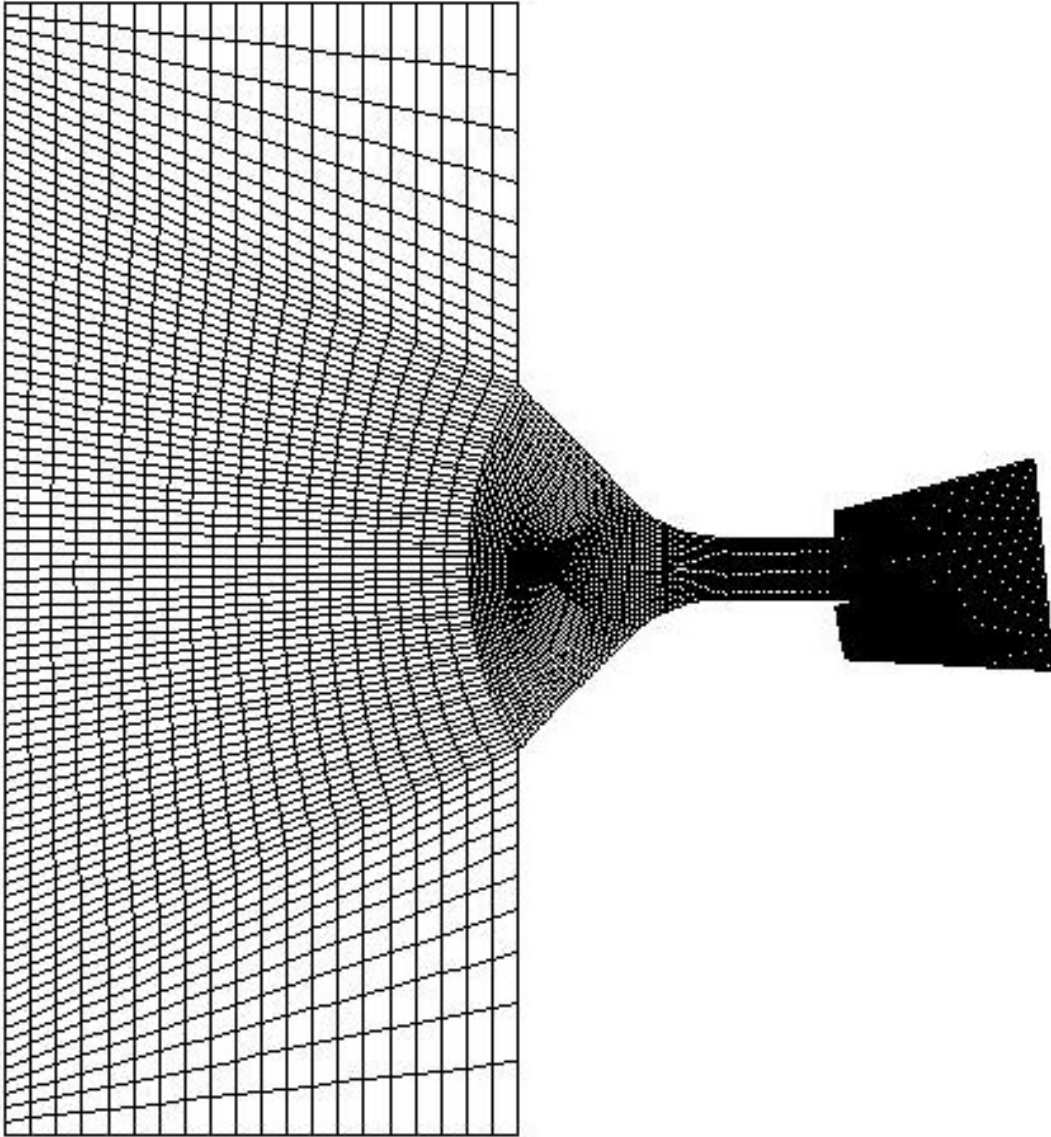


Figure 14. Overview of the grid in case 1. The grids in cases 2 – 7 look the same from above

The seven slightly different grids are all built up of 653,055 cells. They differ only because of the fact that changes in water elevation brings about changes in the flow discharge. The grid in the reservoir is finest close to the water surface and that's why the finest mesh in the reservoir can be found at lower elevation in case 1 than in case 7 (see Figure 15 and Figure 16).

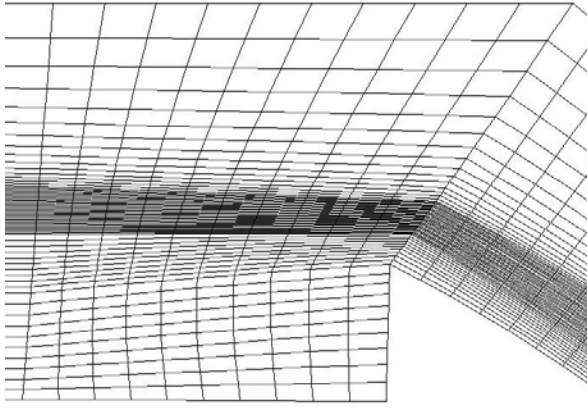


Figure 15. Cut through the hex-mesh in the downstream end of the reservoir and above the spillway crest. The cut is done in the center of the crest. Case 1

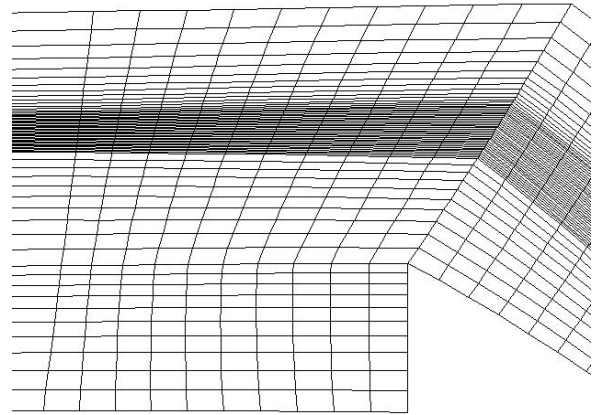


Figure 16. Cut through the hex-mesh in the downstream end of the reservoir and above the spillway crest. The cut is done in the center of the crest. Case 7

Actually, the stilling basin might just as well have been excluded in these cases since the flow in it doesn't affect the flow at the top of the domain; above the spillway crest and in the reservoir.

4 Results and Discussion

This chapter presents the results for the various properties of the flow over the spillway and even some results for the flow in the stilling basin. The hydraulic aspects that are investigated are mainly the discharge capacity of the spillway (cases 1-7), water surface profile along its side walls and the pressure on the spillway chute (cases 6 and 8). In the stilling basin the requested side-wall height and forces on two baffles are studied and even pressure and velocity at the end sill of the basin (case 9).

4.1 Discharge Capacity

The relationship between reservoir water level and flow discharge is referred to as the discharge capacity of the spillway. As for all the other calculations that were done the flow through the bottom outlet is excluded so that the water only passes through the spillway.

Calculations are done for the first seven cases, i.e. for discharge of 50, 100, 150, 200, 250, 300 and 350 m³/s and the head is investigated for each case. The head is defined as the vertical distance from the crest to the unaffected upstream water stage. The results are given in Figure 17 below.

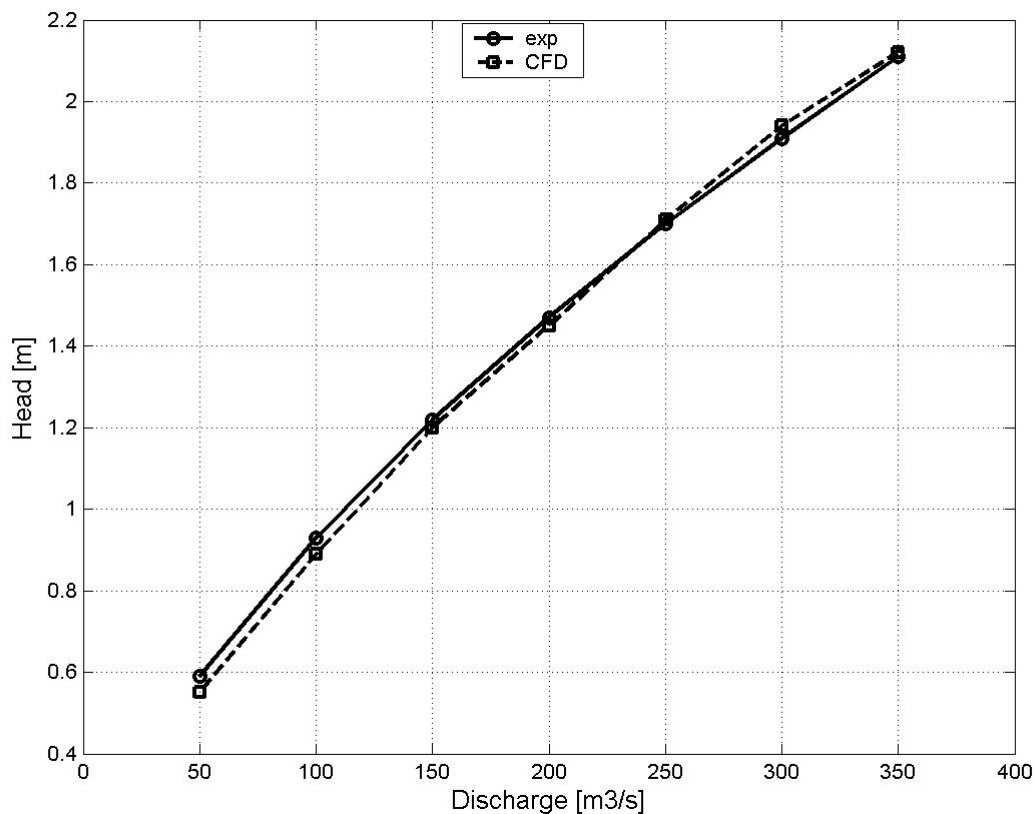


Figure 17. Water level elevation function of flow discharge

The figure shows a good agreement between the experimental and the computed values. The discharge coefficient (C) from the correlation $Q = CBH^{\frac{3}{2}}$ (equation 20) is also

investigated and comparison made between experimental results and the computational results. This comparison is presented in Figure 18.

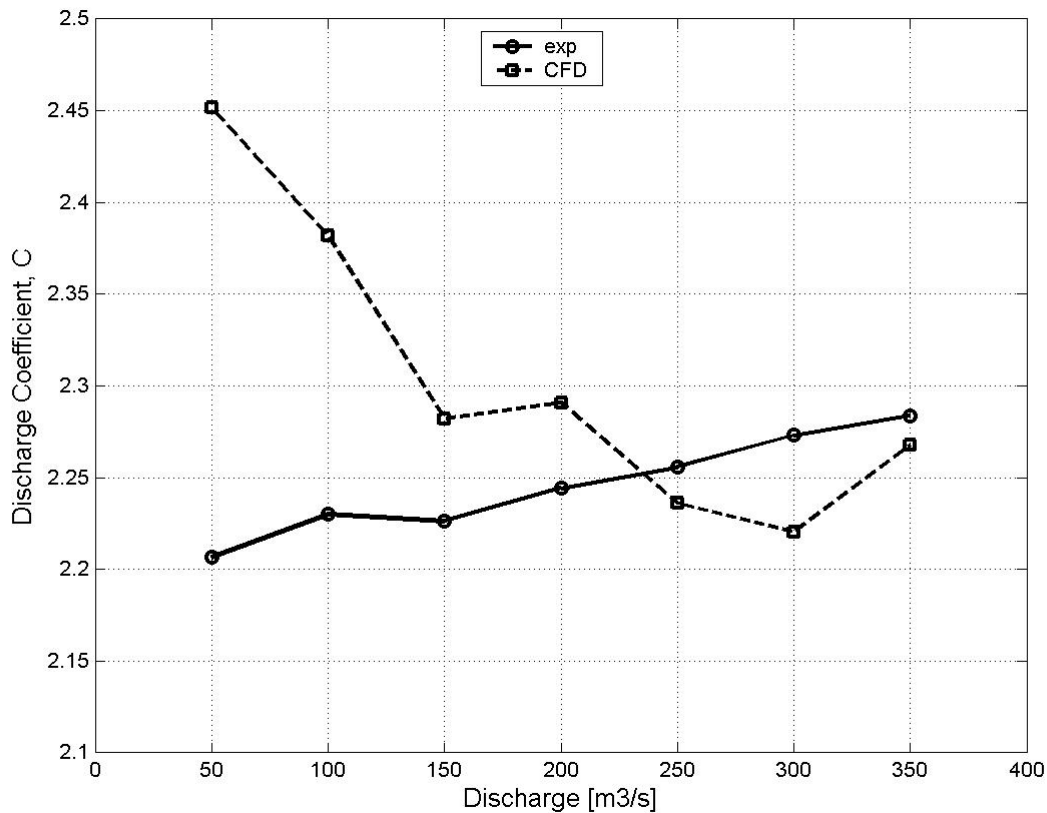


Figure 18. Discharge coefficient function of flow discharge

The largest deviation is evident in case 1, the case with the flow discharge of 50 m³/s. Since the deviation in that case is only around 11 % it can be stated that the agreement between the CFD results and the EXP results is good.

4.2 Water Surface Profile along Side Walls

In two cases (nr. 6 and nr. 8) the water surface profiles are investigated along the transition side walls from the spillway crest to the chute cover. Nine cross sections are chosen for this purpose and the results presented in Figure 19 along with the experimental results. It should be noted that the water depth refers to the flow depth measured perpendicular to the chute bottom but not to the vertical depth.

The mesh in case 8 was designed to resolve the flow in the spillway funnel and chute (the near-wall refinement can be noticed in Figure 9). The mesh in these parts of the design is on the other hand very coarse in case 6 and therefore the larger deviation from the experimental results for that case is understandable.

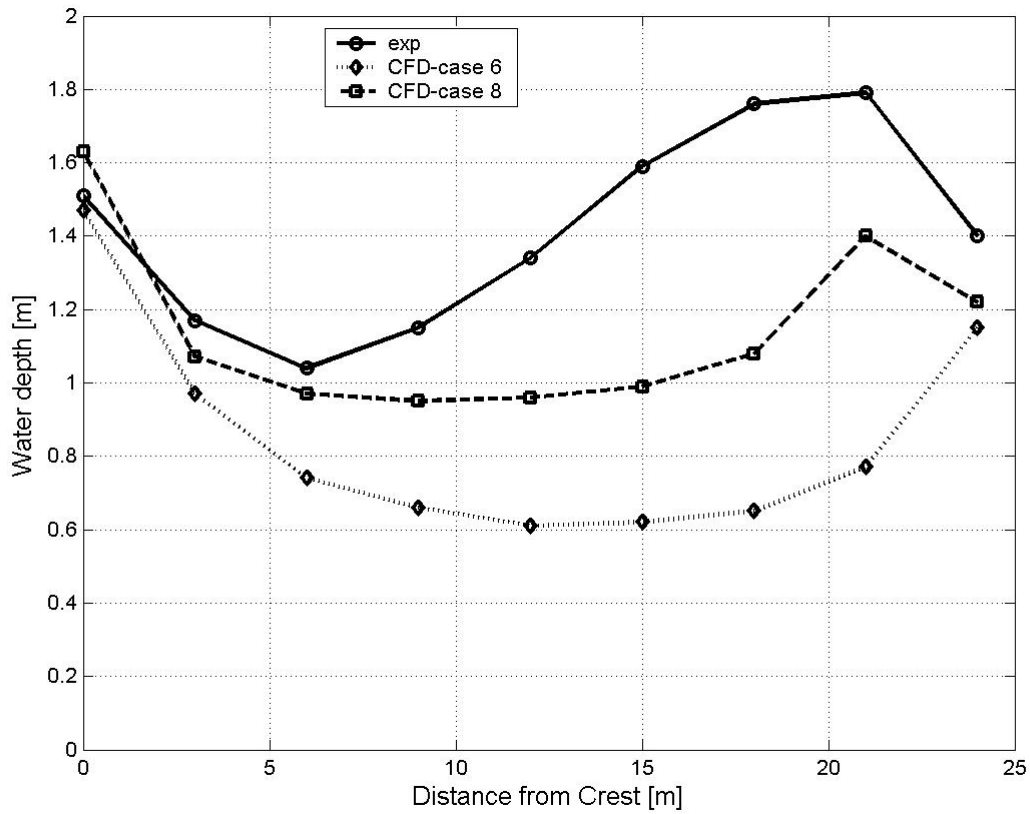


Figure 19. Water surface profile along the side walls comparing results from cases 6 and 8 to the experimental results.

4.3 Pressure on Spillway Chute

In order to investigate the stress on the spillway chute some pressure investigation points were laid down as Figure 20 shows.

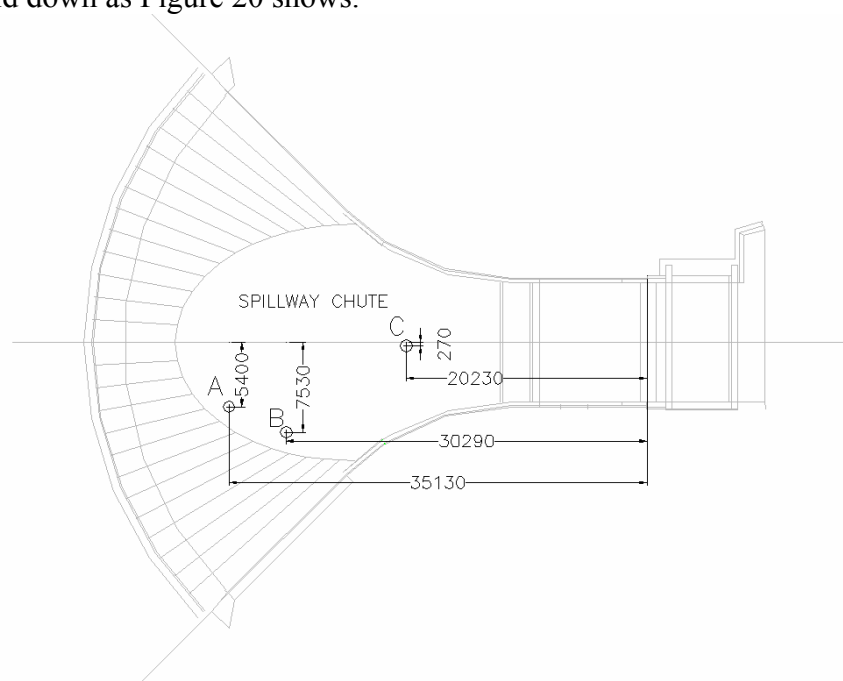


Figure 20. Pressure investigation points in the spillway chute. Dimensions in mm

The pressure investigations are done for case 8; for the flow discharge $300 \text{ m}^3/\text{s}$ and the computational domain restricted to the reservoir and the spillway. The experimental results at four different points from Vattenfall are presented in Table 2 and the computed results compared to them in figures 21– 23.

Table 2. Static pressure acting on spillway chute

Point	A	B	C
Static Gauge Pressure (kPa)	8.59	7.50	37.3

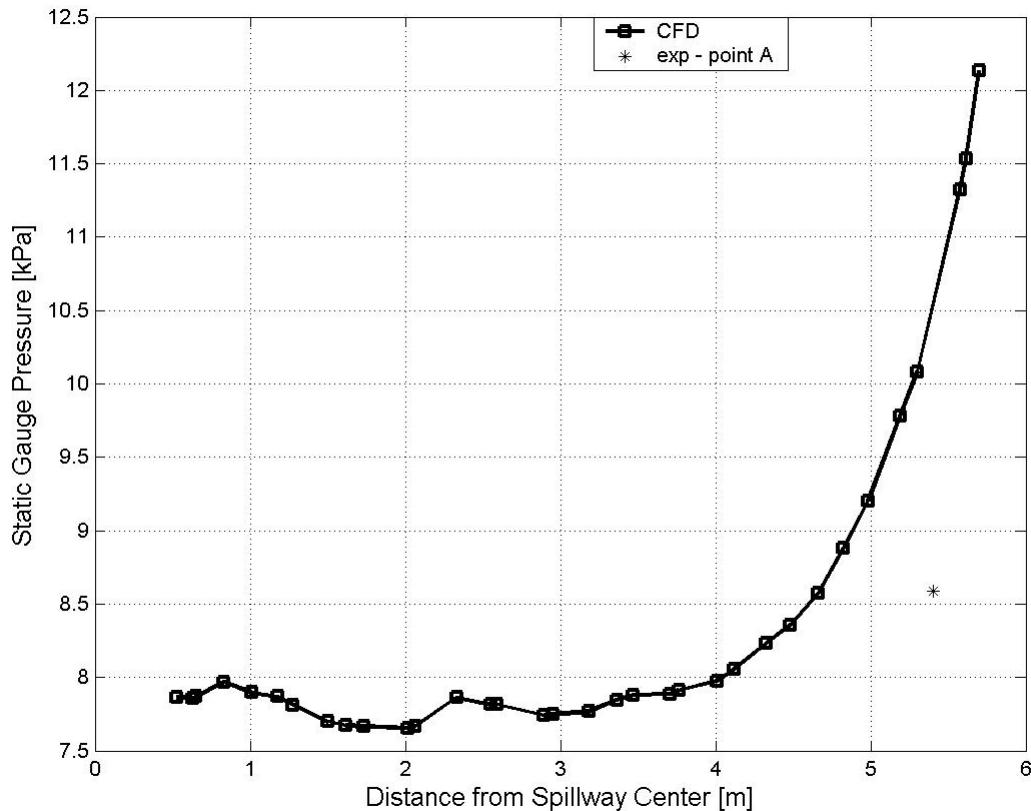


Figure 21. Static gauge pressure function of the distance from the spillway center at the horizontal position of point A (see position in Figure 20)

The calculated values fall fairly close to the experimental value at point A. By interpolating between the calculated values it can be stated that the calculated result deviates by around 23 % from the experimental result. Imprecise geometry used in the CFD calculations must be mentioned as a possible reason for this deviation along with the fact that point A is close to where the spillway chute changes slope.

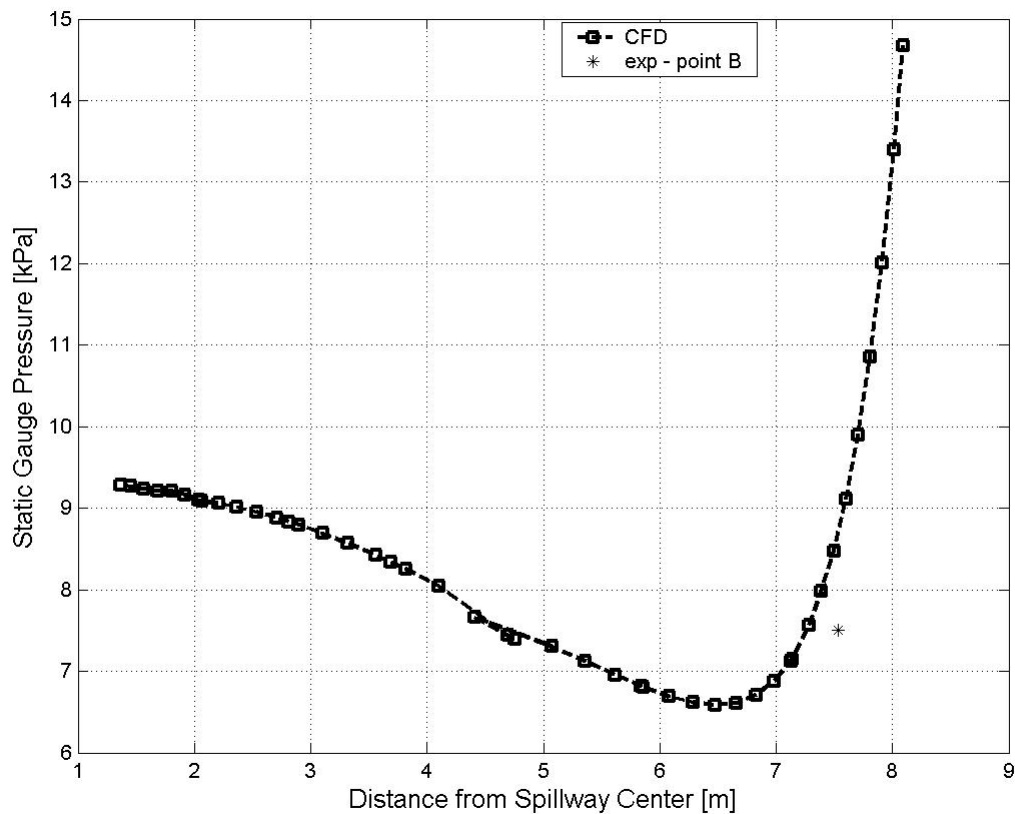


Figure 22. Static gauge pressure function of distance from spillway center at the horizontal position of point B (see position in Figure 20)

For point B the difference between CFD results and experimental results is larger than for point A. Interpolation gives the calculated value 8.7 kPa which deviates by 16 % from the experimental result 7.5 kPa. However, the fact that the experimental value completely fits the CFD results less than 0.5 m closer to the center of the spillway, gives a reason to expect that imprecise geometry is the major reason for the deviation.

The third pressure measuring that was inspected was point C (see Figure 20). The CFD modeling results for the static gauge pressure are presented in Figure 23 along with the experimental value. Interpolation between the CFD values results in 34.0 kPa for point C so the difference between the CFD result and the EXP result (37.3 kPa) is only 9 %. This is interestingly good agreement, especially when the uncertainty in the accuracy of the geometry is kept in mind.

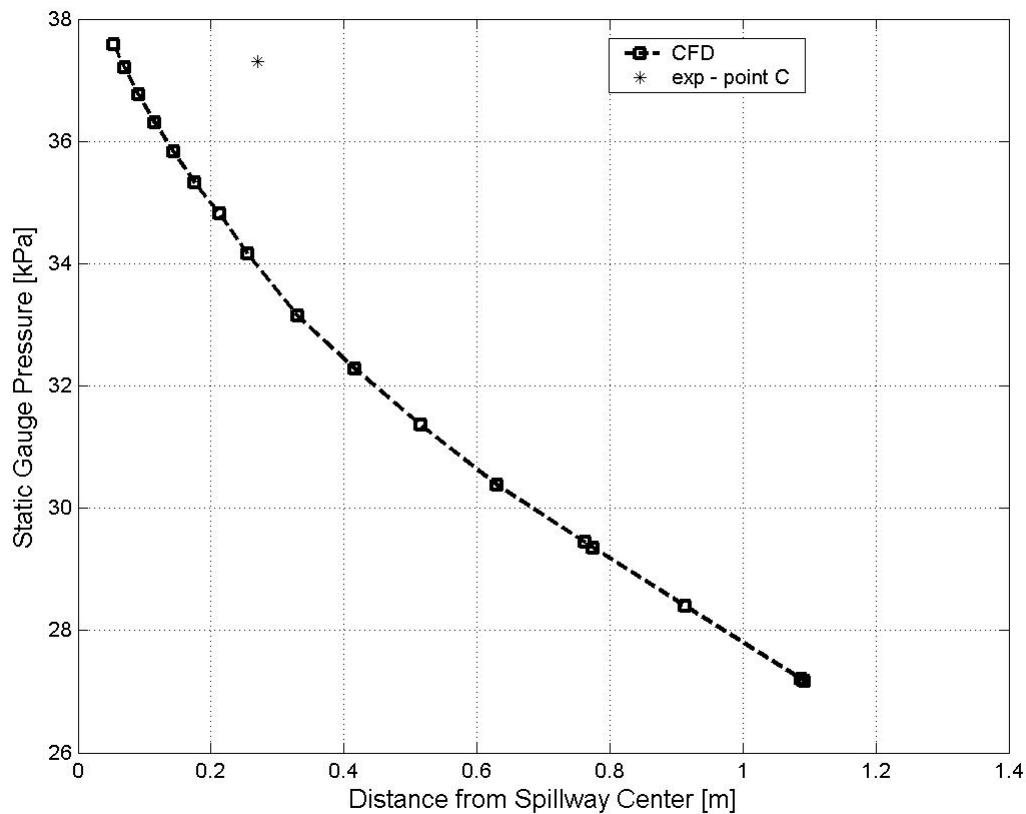


Figure 23. Static gauge pressure function of distance from spillway center at the horizontal position of point C (see position in Figure 20)

4.4 Basin Side-Wall Height

In order to investigate the necessary height of the left side wall of the basin the water surface level was measured in the Vattenfall experiments. This surface level was also investigated in case 9 in the present study and the results compared to the corresponding experimental results in Figure 24. Judging by the figure the computational model does not succeed in calculating the water surface level along the wall. This might be explained by the fact that not all of the rock rip-rap downstream the basin is included in the CFD model. Before including some of the rip-rap in the model (and using the downstream end of the basin as the outlet of the computational domain) even lower water level was achieved along the wall which makes this explanation very likely. Another explanation is grid dependency; the present grid is way too coarse in order to resolve all the turbulent boundary layers along the basin walls.

The hydraulic jump that exists in the stilling basin is a matter of concern in the design of the basin. It is showed in Figure 25 and Figure 26 merely to introduce the possibility of visualizing the water surface in FLUENT.

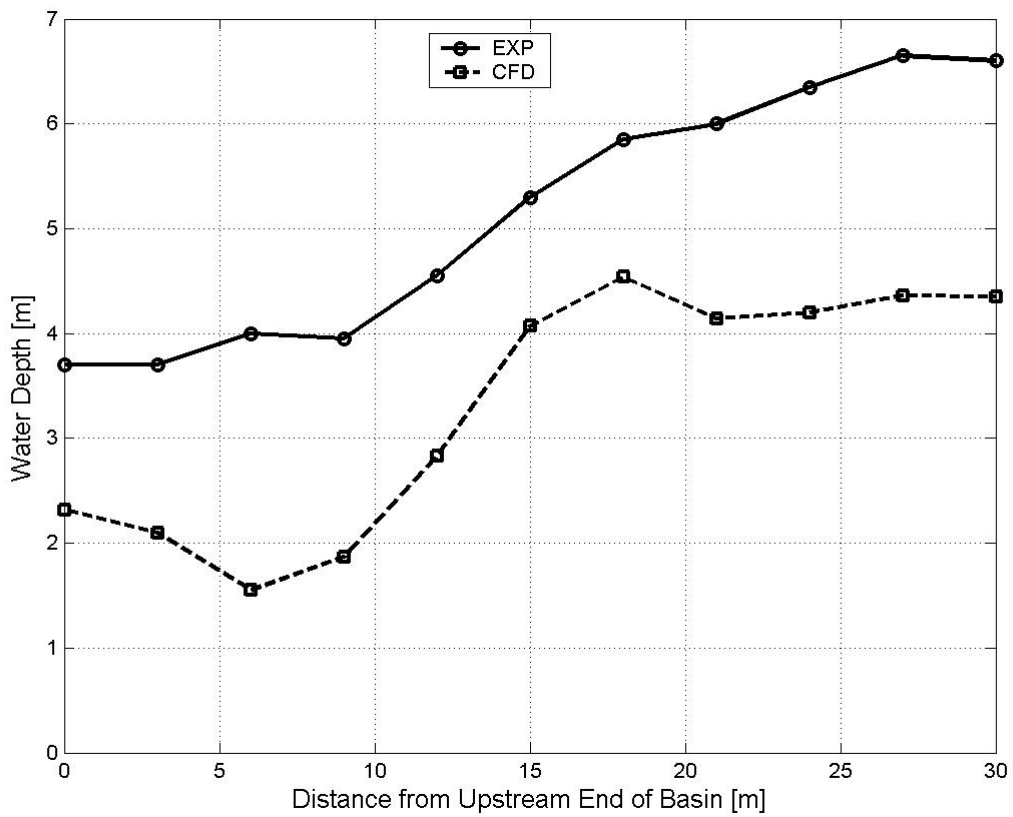


Figure 24. Water depth along the left wall of the stilling basin. Case 9



Figure 25. Water surface in the basin showing a hydraulic jump in the basin with the flow from left to right. The basin walls are not shown and the holes in the spillway bottom are where the baffles are located. Case 9

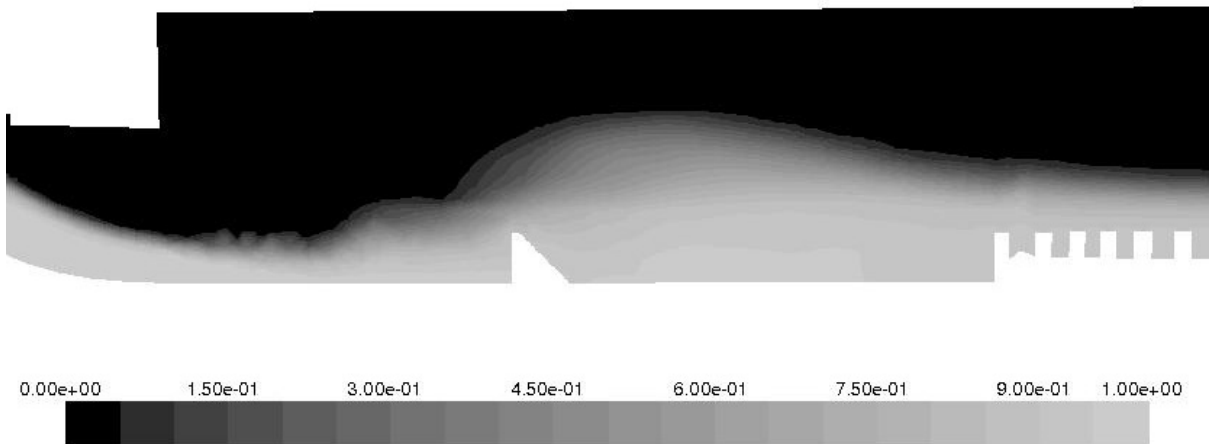


Figure 26. Contours of volume fraction of water in a plane through the middle of the basin. Case 9

4.5 Forces on Baffle Blocks

The pressure on the baffles is a very important property that has got to be taken into account when the baffle blocks are designed. The first row of baffle experiences the highest pressure and therefore the pressure on two baffles of that first row was investigated. Figure 27 shows these two baffle blocks, marked B1 and B2.

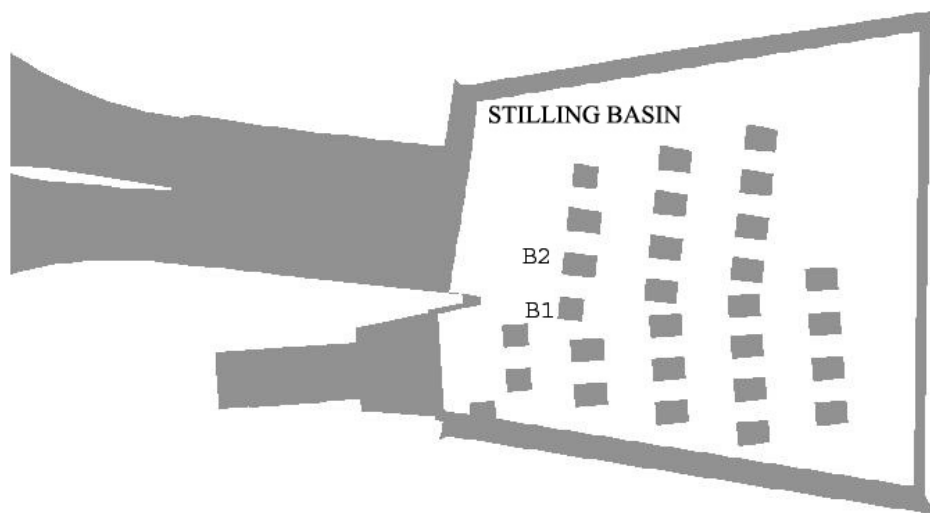


Figure 27. Baffles selected for the pressure investigations in cases 6 and 9

The flow around the baffles can be viewed in a vector plot as in Figure 28 below.

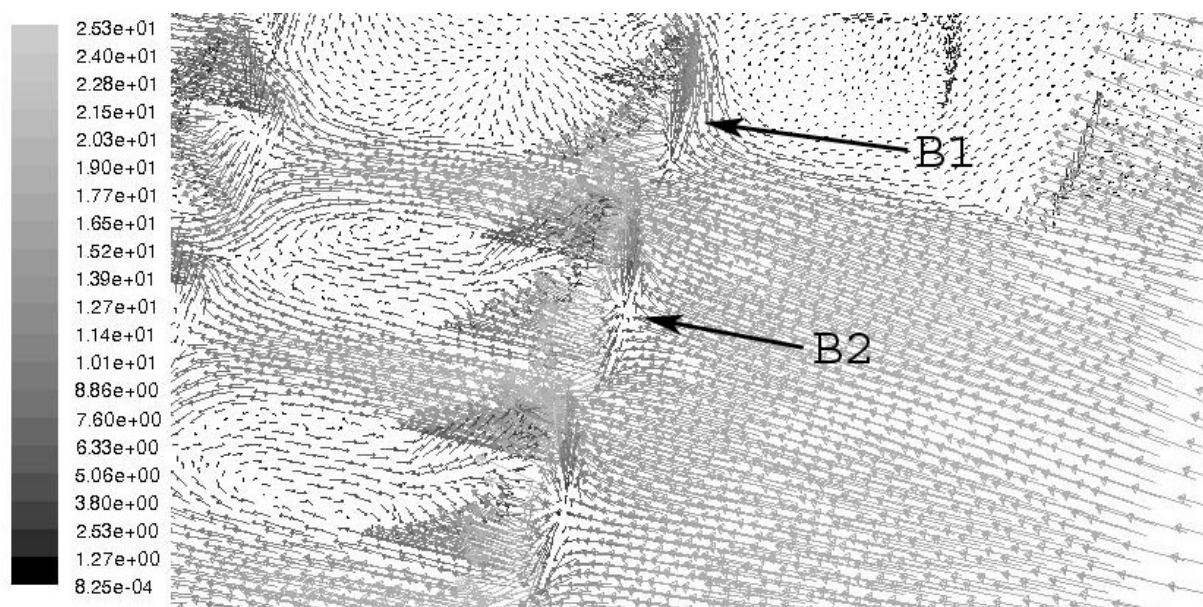


Figure 28. Velocity vectors [m/s] at the basin bottom and around the baffles in the upstream end of the basin seen from above. Case 9

The pressure is investigated on both the upstream face and also on the downstream face of each baffle. The vertical distance from the point on the baffles where the pressure is investigated to the basin floor is given in Table 3.

Table 3. Vertical position of pressure calculation points relative to the basin floor

Baffle	Face (upstream/downstream)	Distance from basin floor (m)
B1	Upstream	0.63
	Downstream	0.65
B2	Upstream	0.83
	Downstream	1.09

The calculated pressure acting on each baffle is presented in Table 4 and compared to experimental values ([1], p. 66).

Table 4. Pressure acting on baffle blocks (gauge pressure)

Baffle	Pressure on upstream face (kPa)	Pressure on downstream face (kPa)	Resultant pressure (kPa)
B1 _{CFD case 9}	151	18	133
B1 _{CFD case 6}	155	1	154
B1 _{EXP}	272	-14	286
B2 _{CFD case 9}	199	- 2	201
B2 _{CFD case 6}	200	-11	211
B2 _{EXP}	233	-5	238

In Table 4 the resultant pressure is calculated as the difference between the pressure on the upstream face and the pressure on the downstream face. This is done for case 6 and case 9 and when compared to the experimental results better results are apparently noted in case 6. For baffle B1 the proportional differences between the CFD-results and the measured pressure are 46 % and 53 % in case 6 and case 9 respectively. The corresponding differences for baffle B2 are considerably smaller; 11 % in case 6 and 16 % in case 9. Grid dependency is most likely responsible for better results in case 6 than in case 9 because the tet-mesh in the basin is even coarser in the latter case. A finer grid is necessary in order to better resolve the flow around baffle B1 and in the basin as a whole.

4.6 Pressure Acting on End Sill

The total pressure is investigated at the pressure investigation locations K, L, M and N presented in Figure 29. These pressure investigations are done 1 m above the basin bottom as in the experiments.

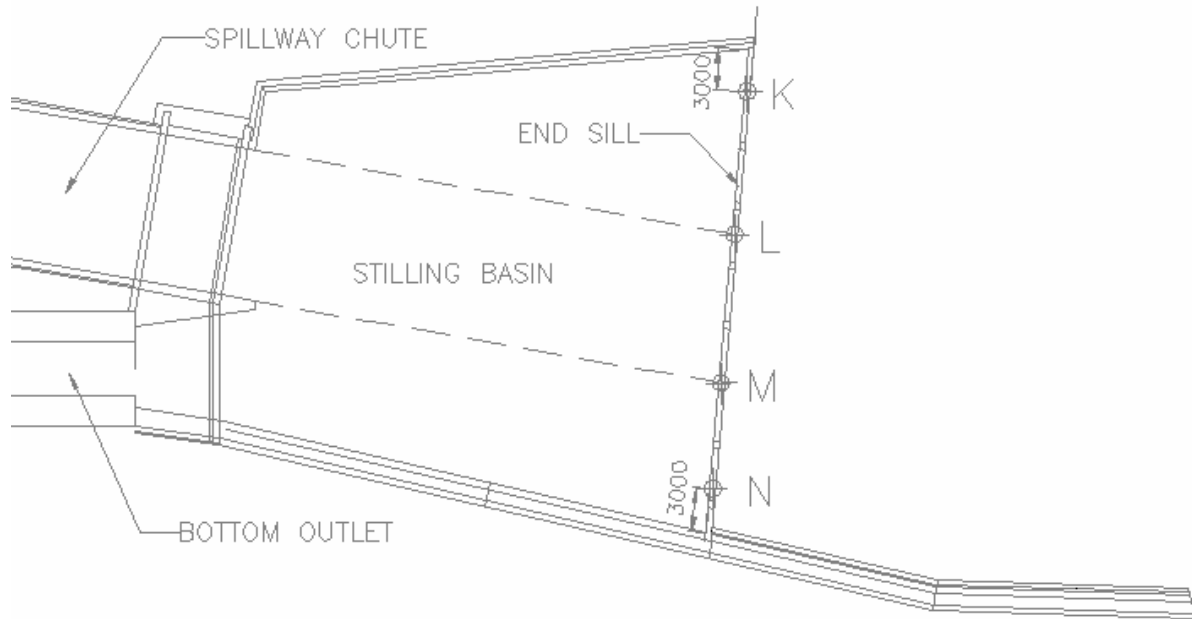


Figure 29. Pressure investigation locations at the end sill. Dimensions in mm. Case 9

Table 5. Pressure acting on end sill (gauge pressure)

Location	Pressure on upstream face (kPa)	Pressure on downstream face (kPa)	Resultant pressure (kPa)	EXP-results (kPa)
K	32.4	29.2	3.2	2.5
L	35.9	34.3	1.6	8.7
M	31.3	26.6	4.7	3.7
N	29.3	26.2	3.1	0.3

The differences between the CFD results and the EXP results are apparent. Once again, a coarse grid and an imprecise modeling of the rock rip-rap may be mentioned as the crucial reasons and with regard to that the CFD results are quite acceptable.

4.7 Velocity Profile at End Sill

The risk for erosion in the river valley downstream the dam is the main reason for the existence of the energy dissipating stilling basin. The spatial stilling basin is ca. 33 m long and its width increases from 22 m at the upstream end to 33 m at the downstream end. The height of the end sill is 2 m.

To judge the risk of erosion downstream the end sill the velocity is investigated at a cross section at the end sill. The velocity is investigated just below the water surface as in the experiments. The velocity distribution is compared to the experimental results (see [4], p. 59) in Figure 30.

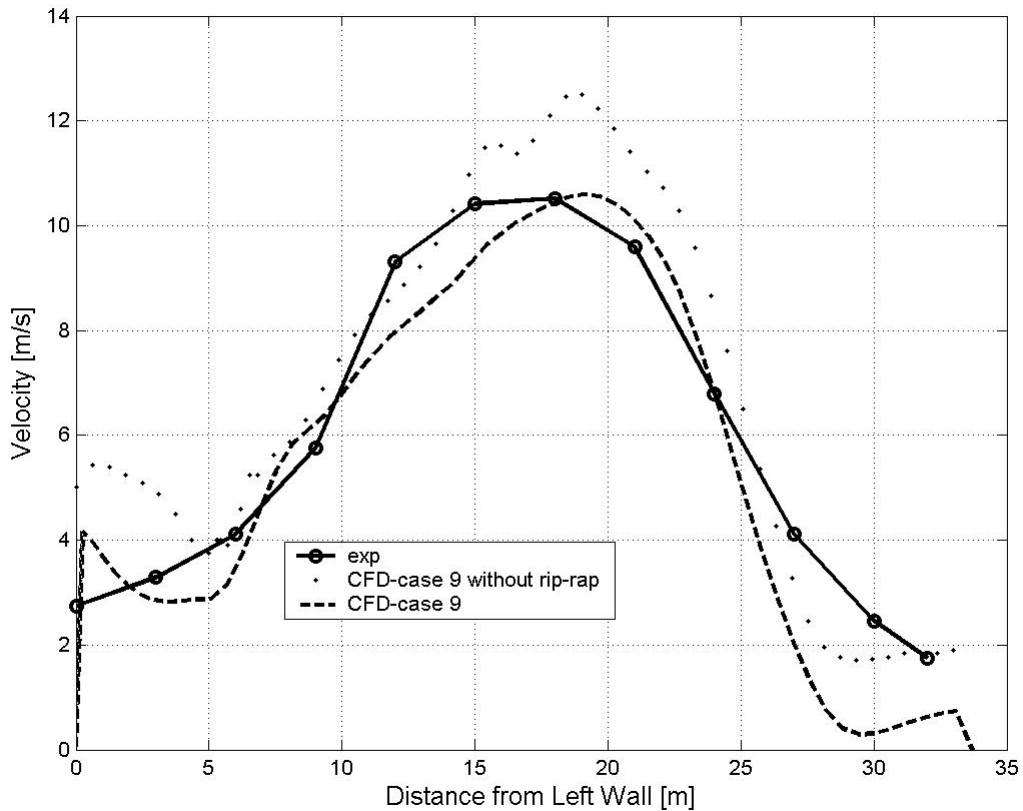


Figure 30. Velocity distribution at the end sill

The figure above compares two CFD-results with the experimental results. The first one was yielded when the rock rip-rap was not included in the model so that the downstream end of the computational domain was the downstream end of the stilling basin. The latter one is from case 9 which has the coarser section of the rip-rap included as earlier described (Chapter 3.5). The results from the former case obviously deviates more from the experimental results judging from the maximum velocity and the general shape of the velocity distribution curve. It should be noted that the level where the velocity is investigated is quite important for the results because the velocity decreases closer to the end sill itself. When the velocity distribution few centimeters above the end sill was checked in the CFD model the maximum velocity was 4.7 m/s compared to 10.6 m/s in case 9 as presented in Figure 30. The experimental result for maximum velocity was 10.5 m/s so it can be stated that the maximum velocity result from case 9 is in very good agreement with that.

5 Conclusions and Future Work

As has already been pointed out the calculations were done on only one desktop computer or one laptop computer. This is the main reason why the computational domain was not refined as well as would have been necessary in order to handle all the complicated flow-phenomena which take place in the flow over the spillway and in the stilling basin. Insufficient grid resolution is especially a problem for all the turbulent boundary layers that do exist in the domain but because of lack of computational power (and limited time) these boundary layers and thereby turbulence is badly resolved. Future work should use much more computational power, and resolve more of the important flow details with a much finer grid. By improving the grid in the stilling basin by using hex-mesh instead of the tet-mesh used in the present study some noticeable gains should be experienced concerning both accuracy and computational power. In spite of all this it may be stated that quite good agreement is yielded between the experimental and computational results for the following aspects: head vs. discharge capacity, pressure in the spillway chute and flow velocity above the basin end sill.

In the very beginning of the project it was decided to restrict the work to flow over the chute spillway and exclude the interesting flow through the bottom outlet. Numerical calculations for flow through the bottom outlet would be very challenging but since this flow situation was a part of the experiments that Vattenfall did some numerical data for comparison already exists. The experiments also covered simultaneous flow over the spillway and through the bottom outlet and that case should also be an interesting, still manageable case for CFD-modeling with FLUENT. Finally, it should be pointed out that doing some research on unsteady (time dependent) flow over the spillway is also possible with FLUENT. An example of what might be achieved with unsteady calculations is the time that it takes to empty the forebay reservoir.

References

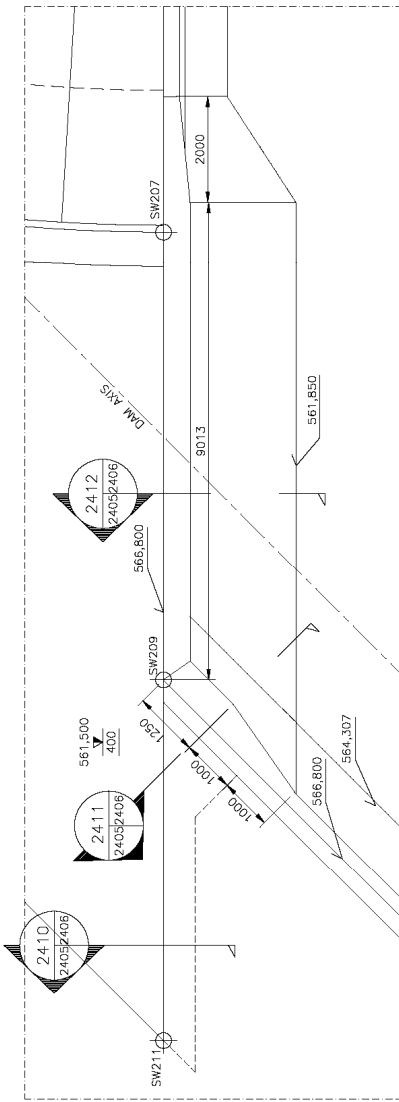
1. FLUENT Manual. www.fluent.com
2. Panton, R. L. 2005. Incompressible flow. John Wiley & Sons, Inc. USA.
3. Stefánsson, Friðberg and Yang, James. 2006. Vatnsfell dam, Iceland – experimental study of flood discharge structures. International Conference HYDRO 2006, Greece.
4. Yang, James. 1999. Vatnsfell hydropower project, Iceland – Hydraulic model studies of flood discharge structures. Vattenfall Utveckling Report serial No. US 99:8. Sweden.

Appendix A

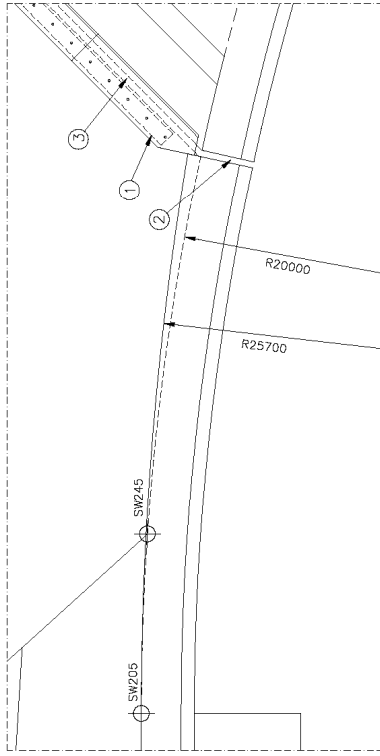
Layout of Vatnsfell Spillway and Connected Structure

Drawings:

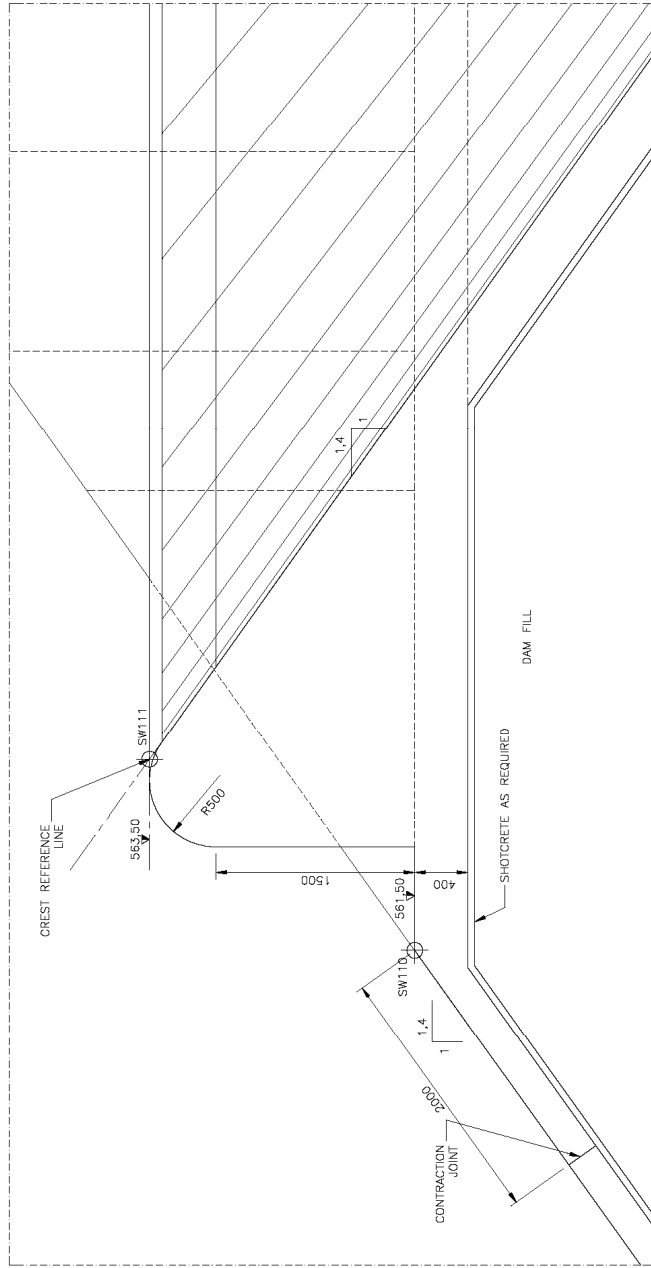
- C-13-0601 General layout
- S-14-2400 Spillway. Overview
- S-14-2401 Spillway. Longitudinal section
- S-14-2405 Spillway. Crest. Details and sections
- S-14-2406 Spillway. Transition wall. Sections
- S-14-2007 Spillway. Chute cover. Details and sections
- S-14-2008 Spillway. Retaining walls. Sections
- S-12-2300 S-Stillling basin. Plan view
- S-12-2301 Stilling basin. Right retaining wall and end sill
- S-12-2302 Stilling basin. Right retaining wall. Sections and details
- S-12-2303 Stilling basin. Left wall and sill. Sections and details
- S-12-2311 Stilling basin. Baffle blocks. Type A and B. Sections and details
- S-12-2312 Stilling basin. Baffle blocks. Type C and D. Sections and details
- S-12-2313 Stilling basin. Baffle blocks. Type E and F. Sections and details
- S-12-2320 Stilling basin. Cut of baffles 2 and 4. Sections and details



2410 DETAIL
2400/2405 SCALE 1



2413 DETAIL
2400/2405 SCALE 2



2409 DETAIL
2401/2405 SCALE 2

NOTATION:

- ① JOINT SHIELD, HOT-DIP GALVANIZED STEEL F1.2. FOR DETAILS SEE METALWORK DWG. M-14-9296.
- ② CONSTRUCTION JOINT IN RETAINING WALL, FOR DETAILS SEE SECTION 2418 ON DWG. -2409.
- ③ CONSTRUCTION JOINT IN BOTTOM SLAB, FOR DETAILS SEE SECTION 2408 ON DWG. -2409.

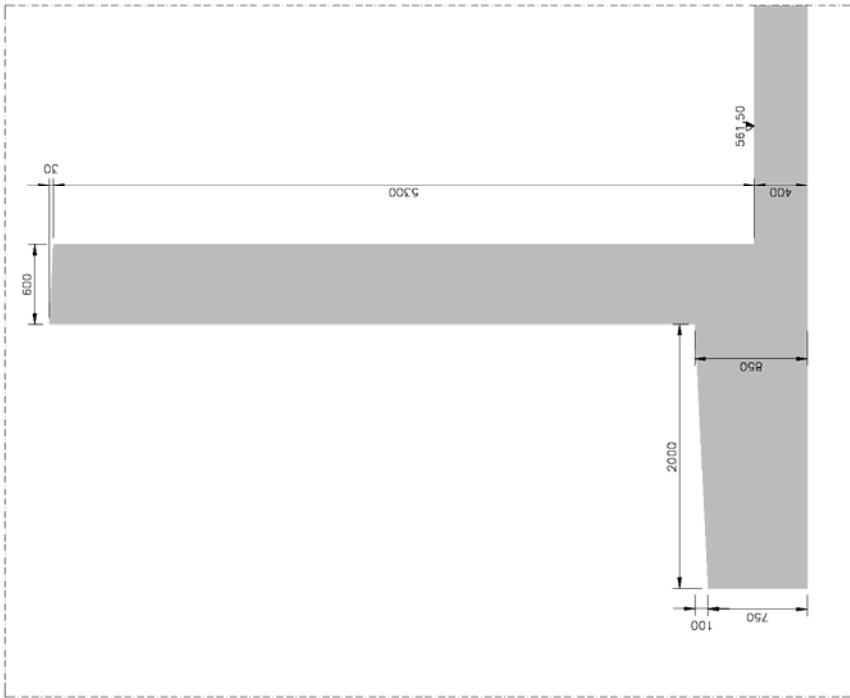
NOTES

- 1. FOR OVERVIEW, SEE DRAWING -2400.
- 2. SEE DRAWING -2400 FOR COORDINATES.
- 3. ALL WATERSTOP JOINTS ARE TO BE WELDED SO AS TO FORM A CONTINUOUS WATER-TIGHT DIAPHRAGM.
- 4. SURFACE FINISH F1 APPLIES TO FORMED SURFACE CONCEALED FROM VIEW, INCLUDING SURFACE UPON OR AGAINST WHICH BACKFILL OR CONCRETE IS TO BE PLACED. FORMED SURFACES OF EXTENSION JOINTS AND BLOCKOUT.
- 5. SURFACE FINISH F2 APPLIES TO FORMED SURFACES EXPOSED TO VIEW, INCLUDING INSIDE SURFACE OF RETAINING WALLS.
- 6. SURFACE FINISH F3 APPLIES TO FORMED SURFACES IN WATERWAYS.
- 7. SURFACE FINISH U1 APPLIES TO UNFORMED SURFACES TO BE COVERED BY FILL OR CONCRETE.
- 8. SURFACE FINISH U2 APPLIES TO UNFORMED SURFACES NOT PERMANENTLY COVERED BY FILL OR CONCRETE.
- 9. SURFACE FINISH OF FACE SLAB SHALL BE EXECUTED AS SOON AS THE CONCRETE SURFACE IS EXPOSED. FINISH SHALL BE BEFORE THE REQUIRES FINISH IN CONCRETE FACE SHALL BE EQUIVALENT TO CLASS F2.
- 10. PROVIDE 25x25 TYPICAL CHAMFER AT ALL EXPOSED CORNERS.

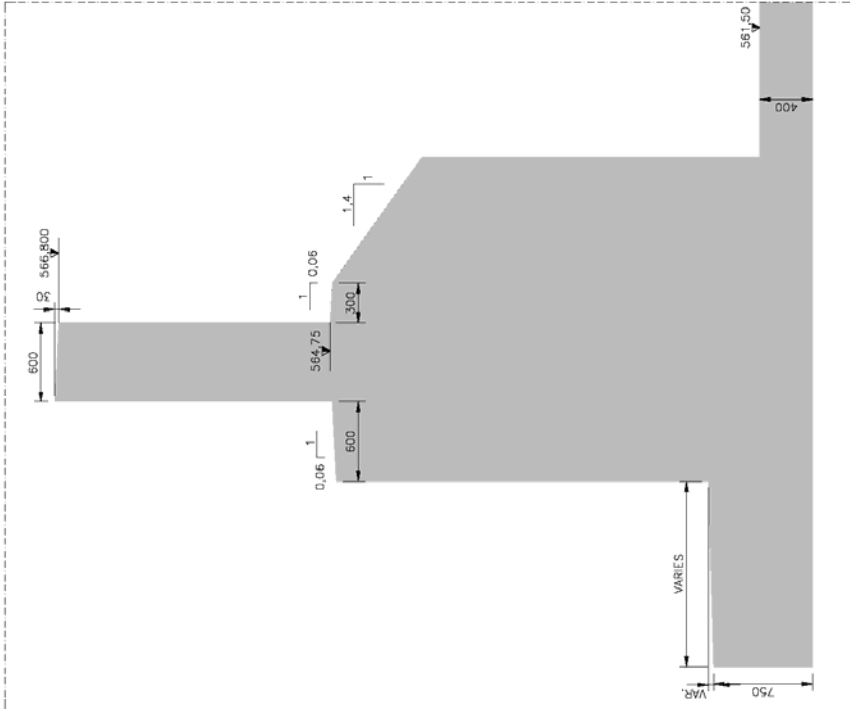
REYNDARTEIKNING
AS BUILT
Ffr. verkkaupa: _____ dags.
Ffr. hömudur: _____
Hömun. VSt. Rafrömun. Glárna-Kín.

REV.	DESCRIPTION	DATE	DES.	CHK.	APP.	DATE	DES.	CHK.	APP.	DATE	REV.	DESCRIPTION
						03.05.2001	FS	ÖJ	ÖJ	03.05.2001	C3	AS BUILT
							FS				C2	ON HOLD REMOVED
						30.01.2001	FS	ÖJ	ÖJ	30.01.2001	C1	ISSUED FOR CONSTRUCTION

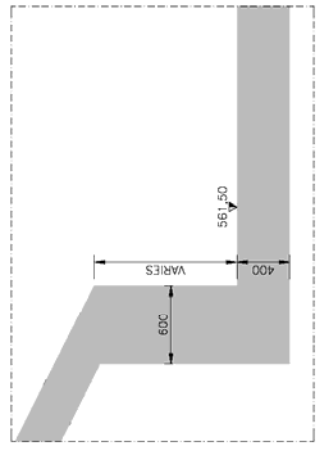
GLAMA · KIM	RAFRÖMUNN	VST	hönnun hf
LANDSVIRKJUN The National Power Company		SPILLWAY, CREST CONCRETE FORMWORK, DIMENSIONS DETAIL AND SECTION	
REV.	NO.	DATE	BY
		5.31.212	REN
S-14-2405			C3



2412 SECTION
24052408 SCALE 1



2411 SECTION
24052408 SCALE 2

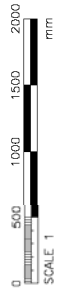


2410 SECTION
24052408 SCALE 1

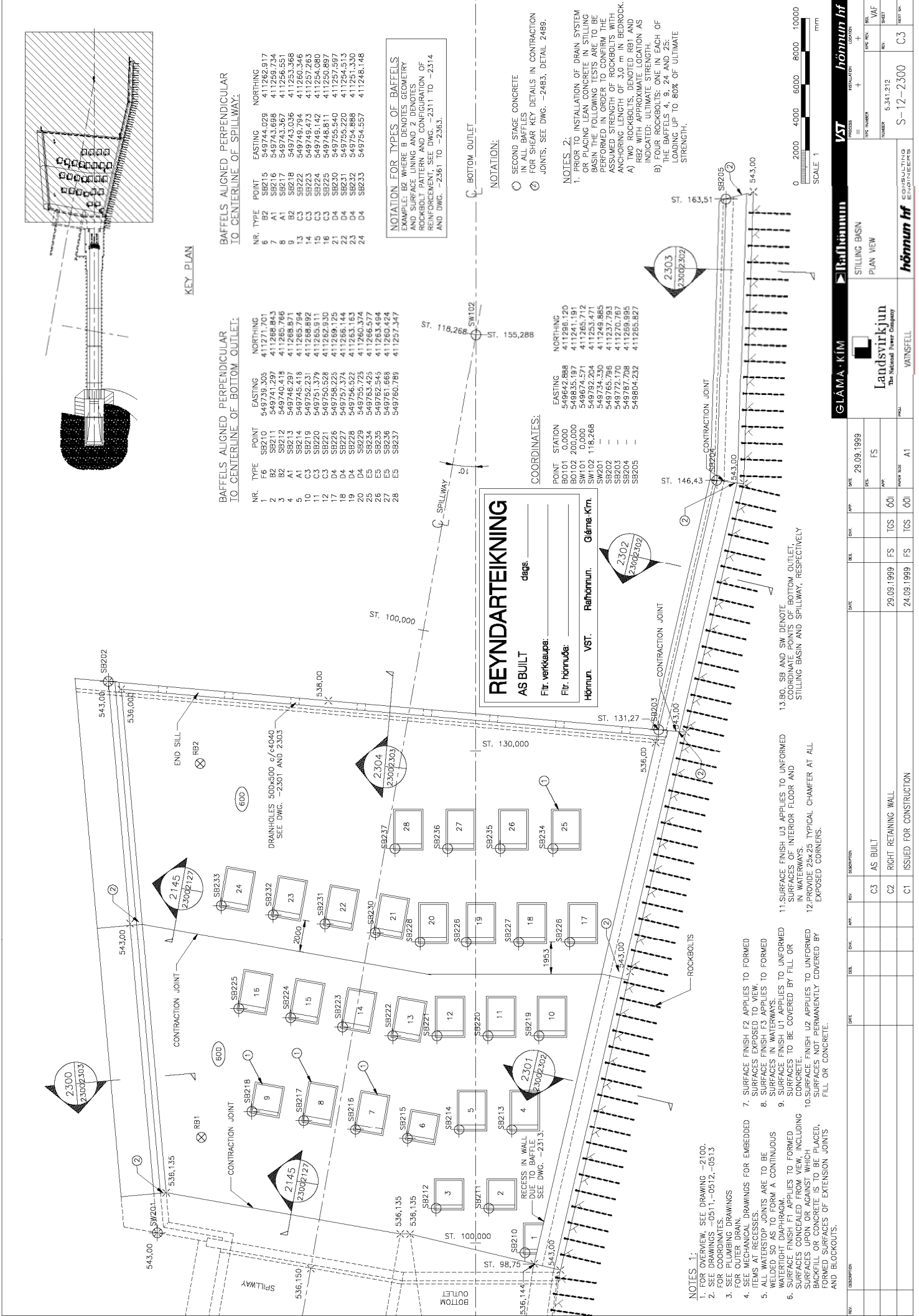
NOTES

1. FOR OVERVIEW, SEE DRAWING -2400.
2. SEE DRAWING -2400 FOR COORDINATES.
3. ALL WATERSTOP JOINTS ARE TO BE WELDED SO AS TO FORM A CONTINUOUS WATERTIGHT DIAPHRAGM.
4. SURFACE FINISH F1 APPLIES TO FORMED SURFACE CONCEALED FROM VIEW, INCLUDING SURFACE UPON OR AGAINST WHICH BACKFILL OR CONCRETE IS TO BE PLACED, FORMED SURFACES OF EXTENSION JOINTS AND BLOCKOUT.
5. SURFACE FINISH F2 APPLIES TO FORMED SURFACES EXPOSED TO VIEW, INCLUDING INSIDE SURFACE OF RETAINING WALLS.
6. SURFACE FINISH F3 APPLIES TO FORMED SURFACES IN WATERWAYS.
7. SURFACE FINISH U1 APPLIES TO UNFORMED SURFACES TO BE COVERED BY FILL OR CONCRETE.
8. SURFACE FINISH U2 APPLIES TO UNFORMED SURFACES NOT PERMANENTLY COVERED BY FILL OR CONCRETE.
9. SURFACE FINISH OF FACE SLAB SHALL BE EXECUTED AS SOON AS THE CONCRETE SURFACE BECOMES APPARENT BENEATH THE SLIPFORM. THE REQUIRED FINISH ON THE CONCRETE FACE SHALL BE EQUIVALENT TO CLASS F2.
10. PROVIDE 25x25 TYPICAL CHAMFER AT ALL EXPOSED CORNERS.

REYNDARTEIKNING
 AS BUILT
 dags. _____
 Ffr. verkeiðkaupa: _____
 Ffr. hönnuða: _____
 Hönnun. VST. Raifhörnun. Gláma-Kím.



GLAMA · KÍM		Raifhörnun		VST		hönnun hf	
Landsvirkjun The National Power Company		SPILLWAY, TRANSITION WALL		CONCRETE FORMWORK, DIMENSIONS		SECTIONS	
REV	DESCRIPTION	DATE	CHK	APP	ISSUED FOR	NO	SECTION
		30.01.2001	FS	ØOI	FOR CONSTRUCTION		
		30.01.2001	FS	ØOI	ISSUED FOR CONSTRUCTION		
		30.01.2001	FS	ØOI	AS BUILT	C2	
		30.01.2001	FS	ØOI	ISSUED FOR CONSTRUCTION	C1	
						FORM NO.	REVISION
						5.341.212	+
						REVISION	+
						NO. REV.	NO.
						S-14-2406	C2
						NO. SHEET	NO. OF SHEETS



BAFFELS ALIGNED PERPENDICULAR TO CENTERLINE OF BOTTOM OUTLET:

NR.	TYPE	POINT	EASTING	NORTHING
1	F6	SB210	549739,306	411271,701
2	B2	SB211	549740,419	411288,843
3	B2	SB212	549740,419	411285,766
4	A1	SB213	549746,297	411288,571
5	A1	SB214	549746,297	411285,716
10	C3	SB219	549752,231	411268,892
11	C3	SB220	549751,379	411265,911
12	C3	SB221	549750,528	411262,930
17	D4	SB226	549758,225	411269,125
18	D4	SB227	549757,374	411266,144
19	D4	SB228	549756,522	411263,163
20	D4	SB229	549755,672	411260,182
25	E5	SB234	549763,425	411266,577
26	E5	SB235	549763,425	411263,600
27	E5	SB236	549761,863	411260,624
28	E5	SB237	549760,789	411257,647

BAFFELS ALIGNED PERPENDICULAR TO CENTERLINE OF SPILLWAY:

NR.	TYPE	POINT	EASTING	NORTHING
6	B2	SB215	549744,029	411262,817
7	A1	SB216	549743,698	411259,734
8	A1	SB217	549743,698	411256,651
9	B2	SB218	549743,036	411253,568
13	C3	SB222	549748,474	411250,765
14	C3	SB223	549748,474	411247,782
15	C3	SB224	549748,142	411254,080
16	C3	SB225	549748,811	411250,897
21	D4	SB230	549755,540	411257,597
22	D4	SB231	549755,220	411254,513
23	D4	SB232	549754,888	411251,330
24	D4	SB233	549754,557	411248,148

NOTATION FOR TYPES OF BAFFELS
 EXAMPLE: B2 WHERE B DENOTES GEOMETRY AND SURFACE FINISH AND 2 DENOTES ROCKBOLT PATTERN AND CONFIGURATION OF REINFORCEMENT. SEE DWG. -2311 TO -2314 AND DWG. -2361 TO -2363.

REYNDARTEIKNING
 AS BUILT
 dags.
 Flr. verkeupa: Gláma-Kím.
 Flr. hönnuð: VST.
 Hönnun: VST. Raðhönnun. Gláma-Kím.

COORDINATES:

POINT	STATION	EASTING	NORTHING
BO101	0,000	549645,888	411294,120
BO102	200,000	549635,197	411241,191
SW101	0,000	549674,571	411265,712
SW102	118,268	549792,204	411253,471
SW201	-	549734,330	411248,885
SB201	-	549765,798	411237,783
SB202	-	549772,170	411220,787
SB204	-	549787,708	411268,995
SB205	-	549604,232	411265,827

- NOTES:
- FOR OVERVIEW SEE DRAWING -2100.
 - SEE DRAWINGS -0511, -0512, -0513 FOR COORDINATES.
 - SEE PLUMBING DRAWINGS FOR OUTER DRAIN.
 - SEE MECHANICAL DRAWINGS FOR EMBEDDED ITEMS AT RECESSES.
 - WELDED STEEL JOINTS ARE TO BE FORMED AS PER A CONTINUOUS WATERFIGHT DIAPHRAGM.
 - SURFACE FINISH F1 APPLIES TO FORMED SURFACES CONCEALED FROM VIEW, INCLUDING SURFACES UPON OR AGAINST WHICH BACKFILL OR CONCRETE IS TO BE PLACED, AND BLOCKOUTS.
 - SURFACE FINISH F2 APPLIES TO FORMED SURFACES EXPOSED TO VIEW.
 - SURFACE FINISH F3 APPLIES TO FORMED SURFACES IN WATERWAYS.
 - SURFACE FINISH U1 APPLIES TO UNFORMED CONCRETE.
 - SURFACE FINISH U2 APPLIES TO UNFORMED SURFACES NOT PERMANENTLY COVERED BY FILL OR CONCRETE.
 - SURFACE FINISH U3 APPLIES TO UNFORMED SURFACES OF INTERIOR FLOOR AND STILLING BASIN AND SPILLWAY, RESPECTIVELY.
 13. SB AND SW DENOTE COORDINATE POINTS OF BOTTOM OUTLET.

GLÁMA - KÍM | Raðhönnun | VST | hönnun hf

STILLING BASIN PLAN VIEW

Landsvirkjun
The National Power Company

VAINSFELL

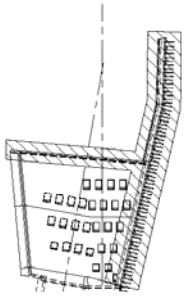
DATE	DESCRIPTION	REV.	APP.	CHK.	DATE
29.09.1999	AS BUILT	C3			29.09.1999
29.09.1999	RIGHT RETAINING WALL	C2			
24.09.1999	ISSUED FOR CONSTRUCTION	C1			

Scale: 1:1000

PROJECT: S-12-2300

DATE: 5.31.2012

REVISION: C3



KEY PLAN

REYNDARTEIKNING

AS BUILT

Fir verkeiðar: deigs

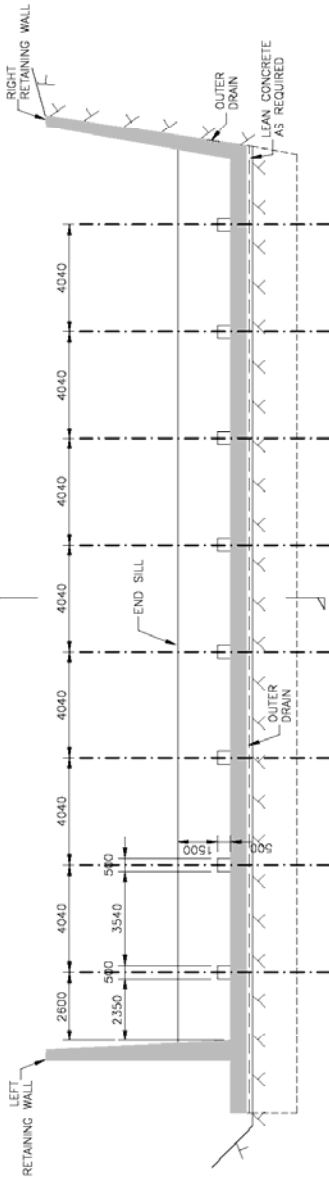
Fir hönnuðar:

Hönnun: VST. Raðhönnun: Gárma-Kfm.

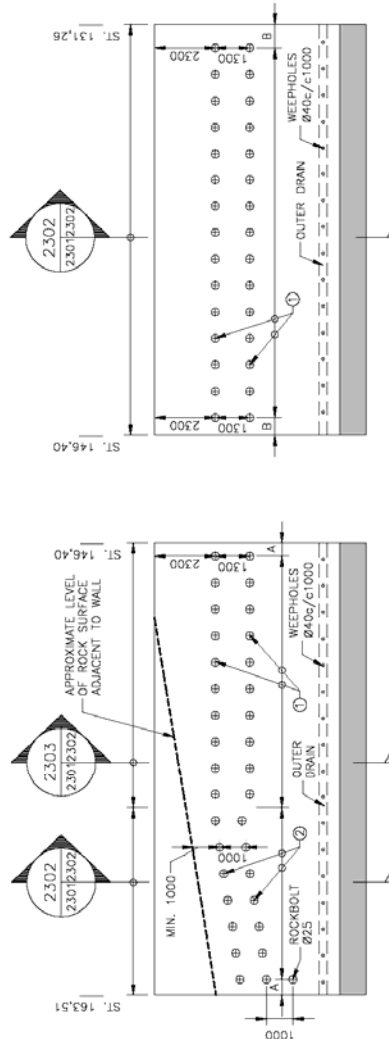
- NOTES:
- FOR OVERVIEW, SEE DRAWING -2100.
 - SEE DRAWING -2300 FOR COORDINATES.
 - SEE PLUMBING DRAWINGS FOR OUTER DRAIN.
 - SEE MECHANICAL DRAWINGS FOR EMBEDDED ITEMS AT RECESSES.
 - ALL WATERSTOP JOINTS ARE TO BE WELDED SO AS TO FORM A CONTINUOUS WATERSTOP.
 - SURFACE FINISH F1 APPLIES TO FORMED SURFACES CONCEALED FROM VIEW, INCLUDING BACKFILL OR CONCRETE IS TO BE PLACED, FORMED SURFACES OF EXTENSION JOINTS AND BLOCKOUTS.
 - SURFACE FINISH F2 APPLIES TO FORMED SURFACES EXPOSED TO VIEW.
 - SURFACE FINISH F3 APPLIES TO FORMED SURFACES IN WATERWAYS.
 - SURFACE FINISH U1 APPLIES TO UNFORMED SURFACES TO BE COVERED BY FILL OR CONCRETE.
 - SURFACE FINISH U2 APPLIES TO UNFORMED SURFACES NOT PERMANENTLY COVERED BY FILL OR CONCRETE.
 - SURFACE FINISH U3 APPLIES TO UNFORMED SURFACES IN INTERIOR FLOOR AND WATERWAYS.
 - PROVIDE 25x25 TYPICAL CHAMFER AT ALL EXPOSED CORNERS.

NOTATION:

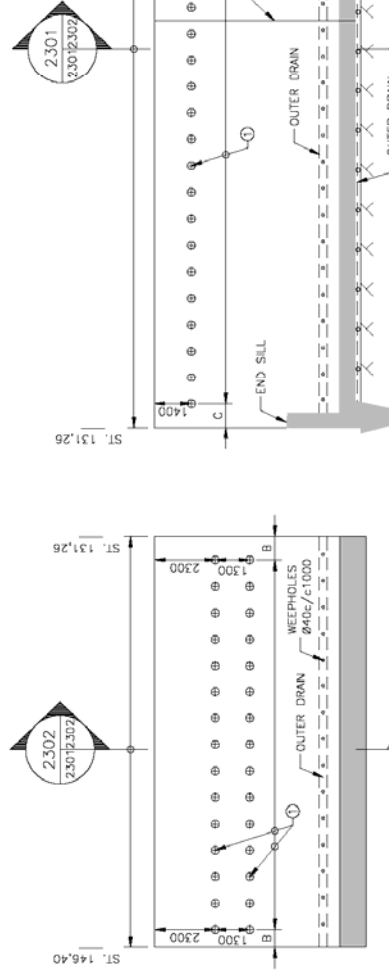
- ① GROUTED ROCKBOLTS Ø20c/c1000-4000 WITH CAP EXTENDING 200mm INTO WALL.
- ② GROUTED ROCKBOLTS Ø25c/c1000-4000 WITH CAP EXTENDING 200mm INTO WALL.



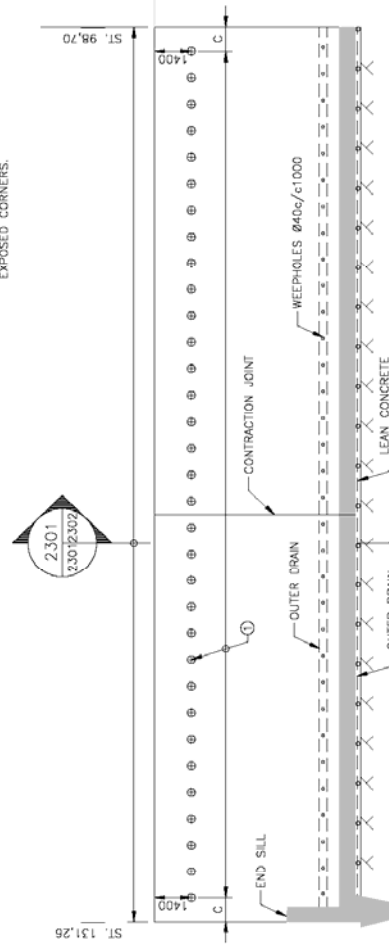
END SILL, SIDE VIEW
SCALE 1



SIDE VIEW, ST. 146.40 - 163.51
SCALE 1



SIDE VIEW, ST. 131.26 - 146.40
SCALE 1



SIDE VIEW, ST. 98.70 - ST.131.26
SCALE 1



GLAMA · KIM Raðhönnun

VST Hönnun hf

Landsvirkjun
The National Power Company

STILLING BASIN,
RIGHT RETAINING WALL AND END SILL
ROCKBOLTS, DIMENSIONS

PROJECT NUMBER: 6.341.212
S-12-2301

REV	DESCRIPTION	DATE	DES.	CHK.	APP.	PRO.	REVISIONS	DATE	BY	CHK.
		24.09.1999	FS							
C2	AS BUILT									
C1	ISSUED FOR CONSTRUCTION									

PROJ. NO.	VAITNSFELL
SCALE	A1
DATE	24.09.1999
DES.	FS
CHK.	
APP.	
PRO.	
TCS	ÖÖI
REV	
DESCRIPTION	
DATE	
DES.	
CHK.	
APP.	
PRO.	
REVISIONS	
DATE	
BY	
CHK.	

NOTES:

1. FOR OVERVIEW, SEE DRAWING -2100.
2. SEE DRAWING -2300 FOR COORDINATES.
3. SEE PLUMBING DRAWINGS FOR OUTER DRAIN.
4. SEE MECHANICAL DRAWINGS FOR EMBEDDED ITEMS AND RECESSES.
5. ALL RECESSES, CUTS AND JOINTS ARE TO BE WELDED, S.W. AS TO FORM A CONTINUOUS WATER-TIGHT DIAPHRAGM.
6. SURFACE FINISH F1 APPLIES TO FORMED SURFACES CONCEALED FROM VIEW, INCLUDING BACKFILL OR CONCRETE IS TO BE PLACED, FORMED SURFACES OF EXTENSION JOINTS AND BLOCKOUTS.
7. SURFACE FINISH F2 APPLIES TO FORMED SURFACES EXPOSED TO VIEW.
8. SURFACE FINISH F3 APPLIES TO FORMED SURFACES IN WATERWAYS.
9. SURFACE FINISH U1 APPLIES TO UNFORMED SURFACES TO BE COVERED BY FILL OR CONCRETE.
10. SURFACE FINISH U2 APPLIES TO UNFORMED SURFACES TO BE PERMANENTLY COVERED BY FILL OR CONCRETE.
11. SURFACE FINISH U3 APPLIES TO UNFORMED SURFACES OF INTERIOR FLOOR AND IN WATERWAYS.
12. PROVIDE 25x25 TYPICAL CHAMFER AT ALL EXPOSED CORNERS.

NOTATION:

- ① GROUTED ROCK BOLTS Ø20c/c1000-4000 WITH CAP EXTENDING 200mm INTO WALL.
- ② GROUTED ROCK BOLTS Ø25c/c1000-4000 WITH CAP EXTENDING 200mm INTO WALL.
- ③ OUTER DRAIN.

REYNDARTEIKNING

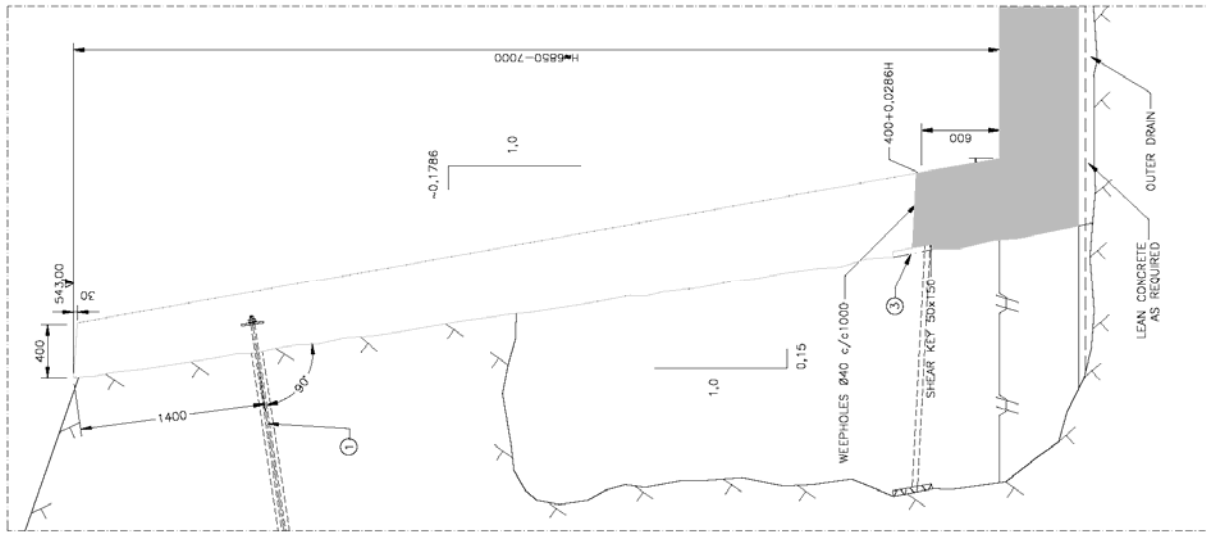
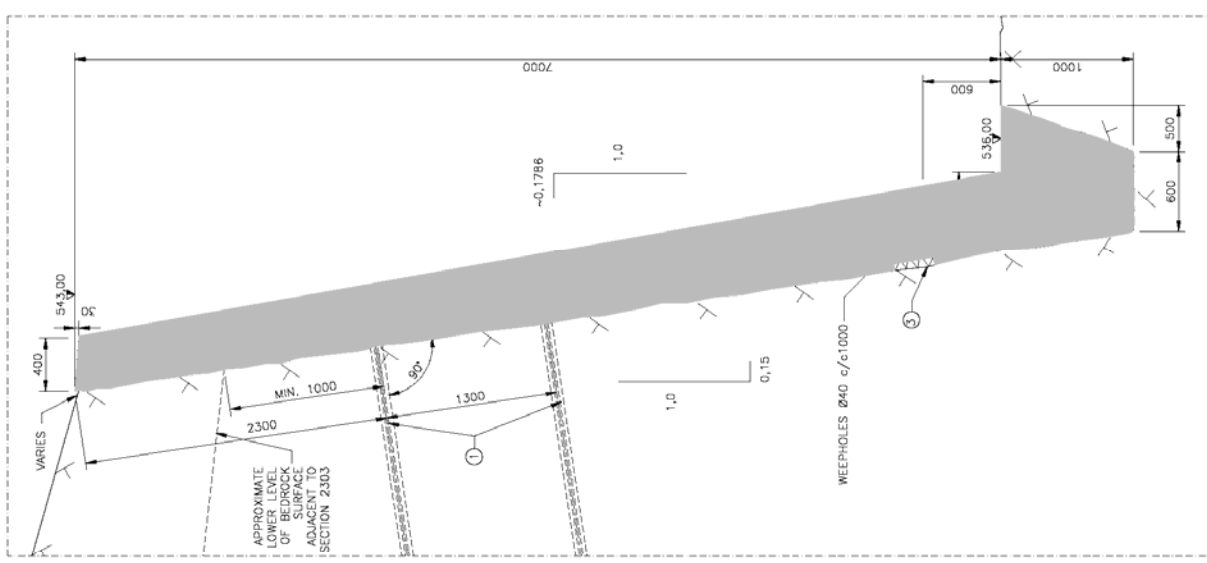
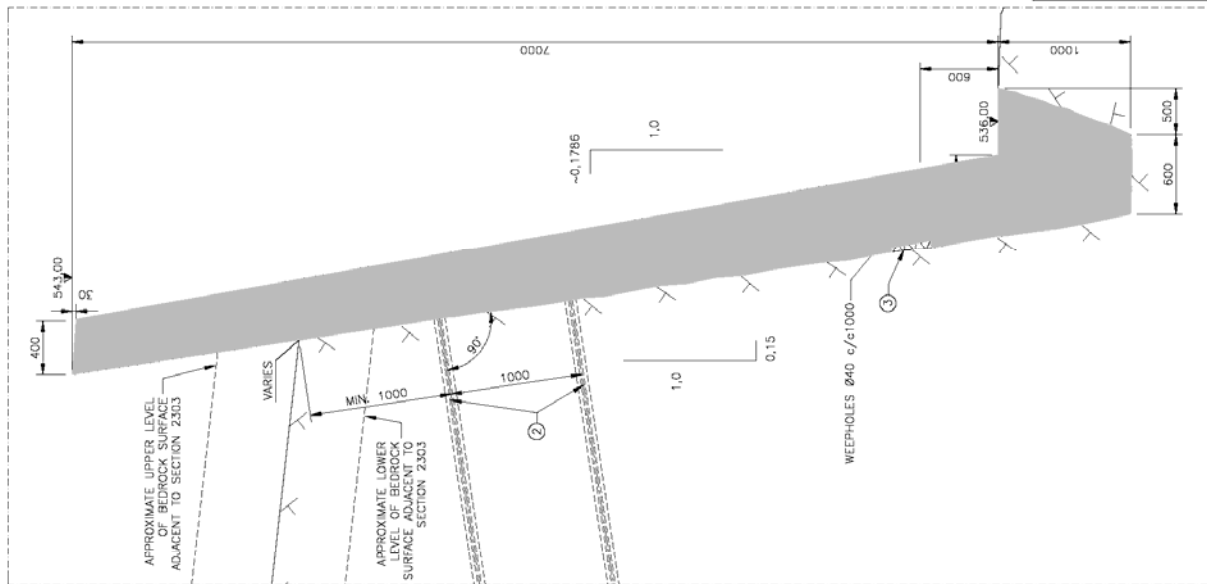
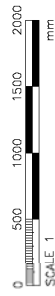
AS BUILT

Flr. verkkaupa:

Flr. hönnuð:

dag:

Hönnun: VST, Reiðhönnun, Gláma-Krín.

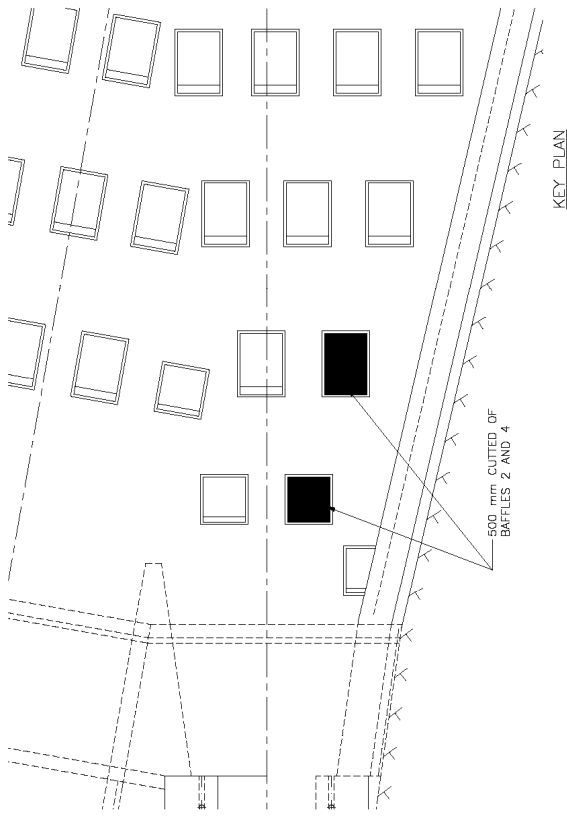
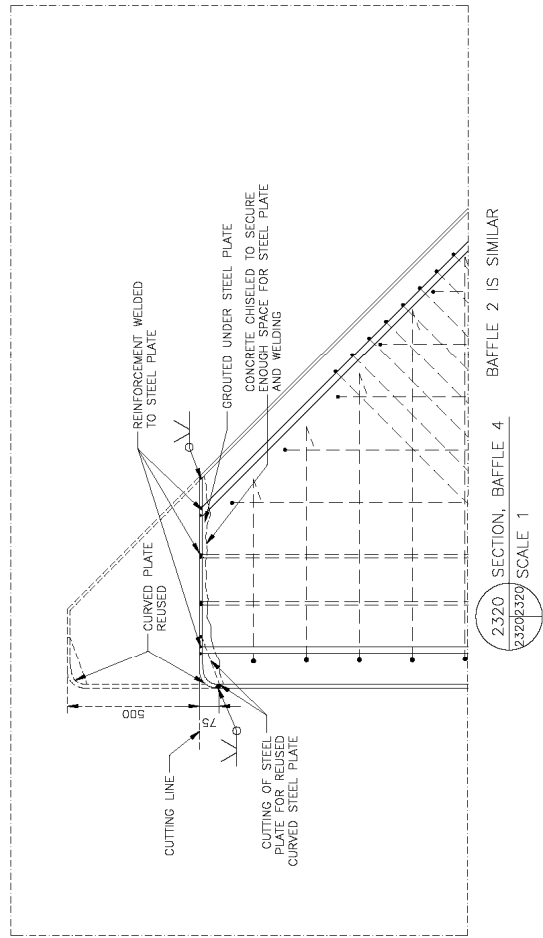
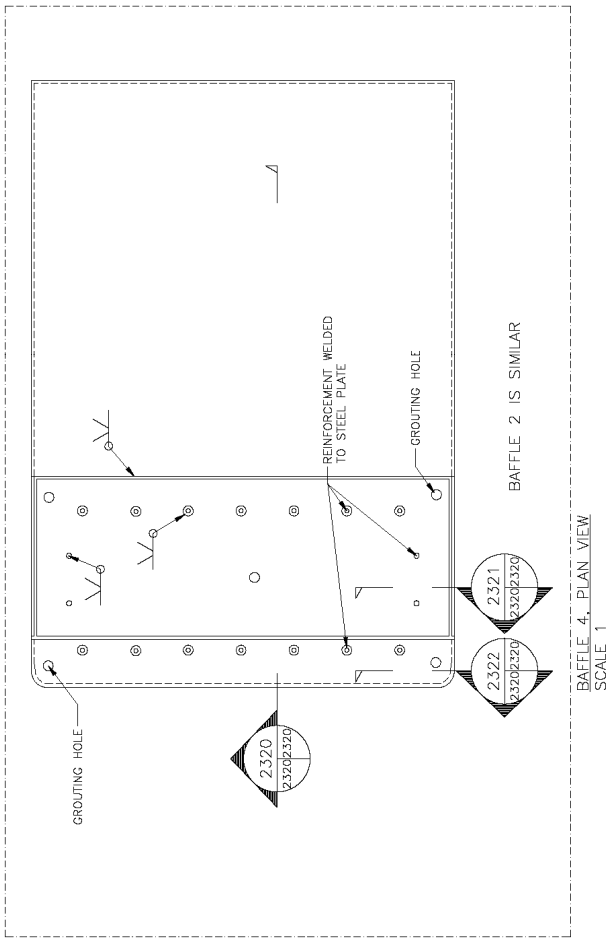


2303 SECTION
23002302/SCALE 1
2301

2302 SECTION
23002302/SCALE 1
2301

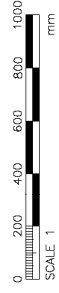
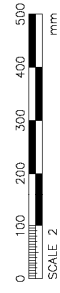
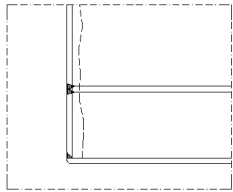
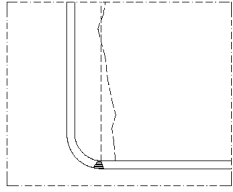
2301 SECTION
23002302/SCALE 1
2301

GLAMA · KÍM		Reiðhönnun		VST		hönnun hf	
Landsvirkjun The National Power Company		VAITNSFELL		CONCRETE FORMWORK, DIMENSIONS SECTIONS AND DETAILS		REVISIONS	
REV	DESCRIPTION	DATE	DES	CHK	APP	REV	DATE
		29.09.1999	FS	TCS	ÓOI	5.34.1.212	REV
		24.09.1999	FS	TCS	ÓOI	S-12-2302	REV
		29.09.1999	FS	TCS	ÓOI	C3	REV
		29.09.1999	FS	TCS	ÓOI	C3	REV



NOTES:

1. 500mm SHALL BE CUTTED OF THE TOP OF BAFFLES 2 AND 4.
2. REINFORCEMENT AT FRONT OF BAFFLES SHALL BE CUTTED EXTRA 75mm FOR REUSED CURVED STEEL PLATE.
3. CONCRETE SHALL BE CHISELED TO SECURE ENOUGH SPACE FOR STEEL COVER AND WELDING OF REINFORCEMENT.
4. STEEL PLATES SHALL BE TRIMMED FOR WELDING GAPS AND WELDED ON PLACE.
5. GROUTING UNDER STEEL COVER SHALL BE DONE WITH NONE SHRINK CEMENT GROUT.



REYNDARTEIKNING
AS BUILT

Fit. verkeupa: _____ dags.

Fit. hönnuða: _____

Hönnun. VST. Ræðhönnun. Gláma-Kím.

REV	DESCRIPTION	DATE	DES.	DRAWN	CHECK	DATE	APP.	DATE	REV.	DESCRIPTION	DATE	APP.	DATE	REV.	DESCRIPTION
C2	AS BUILT					02.07.2002									
C1	ISSUED FOR CONSTRUCTION					02.07.2002									

GLAMA-KÍM	Ræðhönnun	VST	hönnun hf
Landsvirkjun	STILLING BASIN, BAFFLE BLOCKS	TYPE NUMBER	5.34.1.212
Fit. National Paper Company	CUT OF BAFFLES 2 AND 4	REV.	
VATNSHELL	SECTIONS AND DETAILS	REV.	
	hönnun hf	PROJECT	S-12-2320
	ENGINEERS	ISSUED BY	C2

Appendix B

How to Get a Well Resolved Surface with the VOF Method in FLUENT

The purpose of this chapter is to serve as a tutorial for the VOF method in FLUENT for users who are acquainted to FLUENT but not to the VOF method. In order to get a well resolved free surface with the VOF method there are several things that have to be taken care of. Before the complicated case of the spillway and its surroundings was studied, a case of a much simpler spillway was studied (see Figure 31).

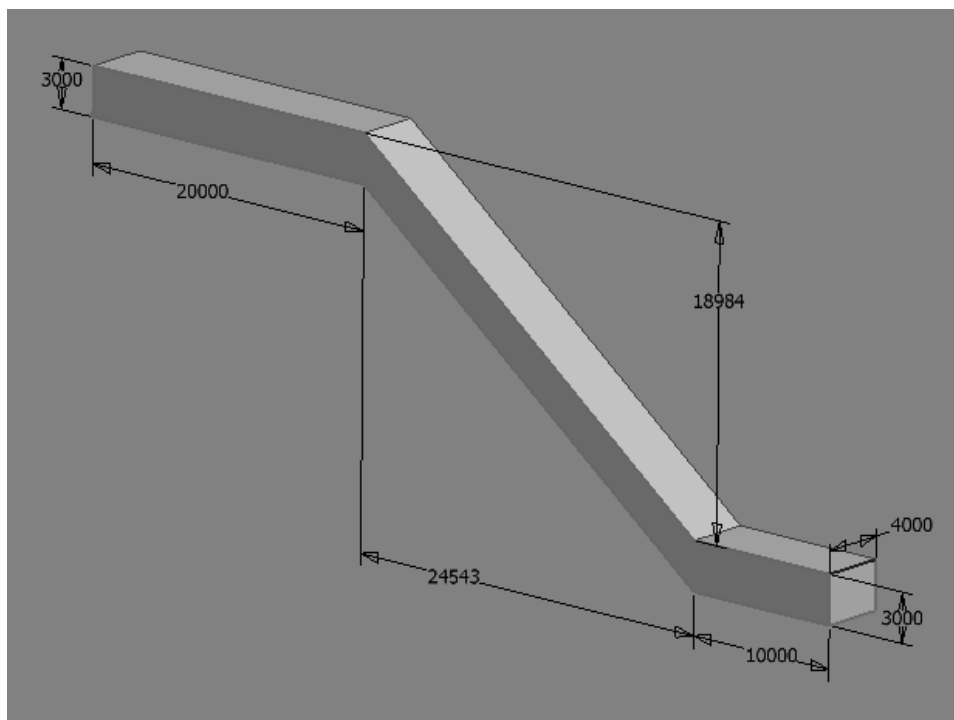


Figure 31. The simple model used for studying the VOF method. Dimensions in mm

After having selected “Volume of Fluid” as the model in the Multiphase Model panel the appropriate VOF scheme was selected and in this case it is the implicit one since the subject is a steady flow. The flow was defined as steady in the Solver panel. The implementation of the standard $k-\epsilon$ turbulence model with standard wall functions was specified in the Viscous panel. The materials were defined in the Materials panel and the possibility to get the properties of the fluids from the Fluent database used.

The two different phases were defined in the Phases panel. Air was defined as the primary phase according to recommendations from the VOF tutorial. When defining the initial solution it is very important to patch an initial position of water in the domain because it increases stability in the calculations. It is easier to patch a water volume fraction of 1 in this rather small volume instead of patching an air volume fraction of 1 everywhere else in the domain so that is why water is more suitable as the secondary phase.

In the Operating Conditions panel the operating pressure of 101325 Pa was set and the reference pressure location was situated in a region where the fluid would at all times be air,

never any trace of the water phase. This was done to ensure smooth and rapid convergence. In this panel gravity was also specified in terms of the x, y and z components of the gravitational acceleration vector. Finally, the density of air, 1.225 kg/m^3 , was specified as the operating density. This is recommended in the Fluent manual in order to exclude the buildup of hydrostatic pressure within the air phase, improving the round off accuracy for the momentum balance.

To reduce the diffusivity in the interface between the two faces (air and water) the modified HRIC discretization scheme was used in all of these pre-VOF-studies. PRESTO! was used as the pressure interpolation scheme and PISO as the pressure – velocity coupling scheme. For all variables under-relaxation is recommended to be set as low as 0.2-0.5 for all steady VOF calculations in order to increase stability. It was found that 0.4 for pressure, density, body forces and momentum and 0.3 for volume fraction, k , ϵ and μ_t were low enough to give stable calculations.

The boundary conditions that were defined were the following:

- the area above the spillway as pressure outlet with
 - backflow I = 10 %
 - backflow $D_H = 50 \text{ m}$
 - backflow volume fraction for water: 0
 - gauge pressure: 0 Pa
- the inlet as mass flow inlet with
 - mass flow of water: 7985.6 kg/s
 - mass flow of air: 4 kg/s
 - I = 5 %
 - $D_H = 12 \text{ m}$
 - open channel boundary condition used with Inlet Group ID set as 1 since both air and water enter through the same inlet, bottom level 0 m and free surface 2 m.
- the outlet as pressure outlet with
 - backflow I = 10 %
 - backflow $D_H = 10 \text{ m}$
 - backflow volume fraction for water: 0
 - gauge pressure: 0 Pa

One of the most important properties of the VOF method is that the interface between the two phases can be judged from the volume fractions of the two phases. The problem is that it has to be decided how specific requirement can be put on the diffusivity of the volume fraction at the interface. While doing this pre-study the requirement is that the elevation of the surface of volume fraction 0.3 does not differ from that of volume fraction 0.7 by more than 3 cm. When this requirement is fulfilled the surface is considered to be presented by the surface of volume fraction 0.5.

The first comparison that was made was between two very rough meshes, one unstructured tet-mesh and one structured hex-mesh. The unstructured mesh was built up of 4778 cells and has an interval size of 1000 mm in each direction (see Figure 32). A cut is made through the center of the domain and the grid showed on that plane. As expected this grid gave very bad results for the contours of volume fraction of water as can be seen in Figure 33-35. The flux report for mass flow rate of the mixture of air and water gave 5.3 kg/s difference between in- and outflow

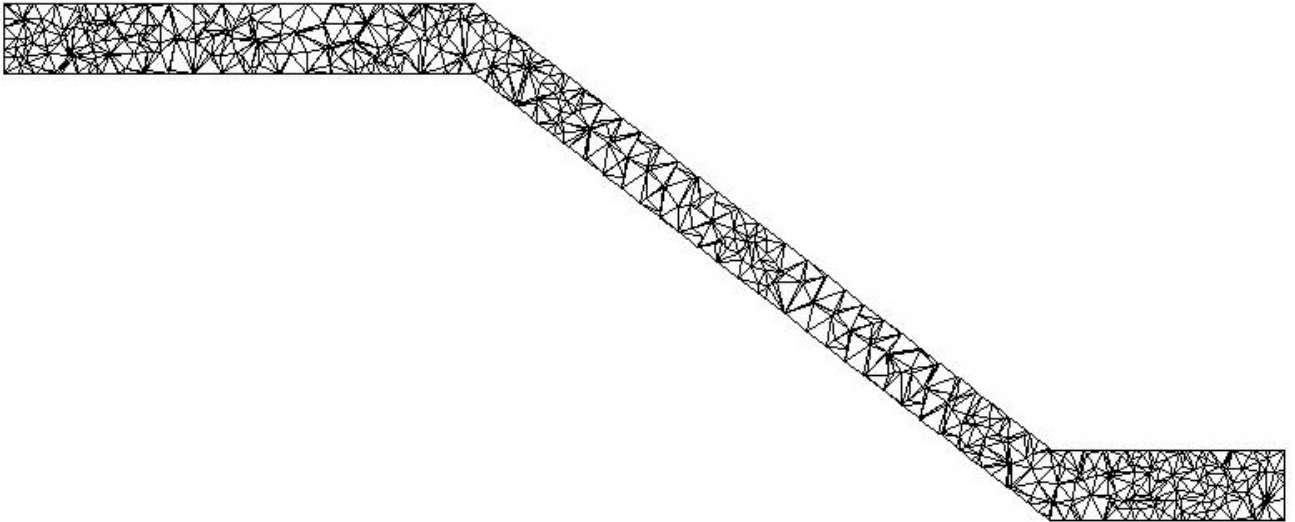


Figure 32. Cut through a tet-mesh of 4778 cells

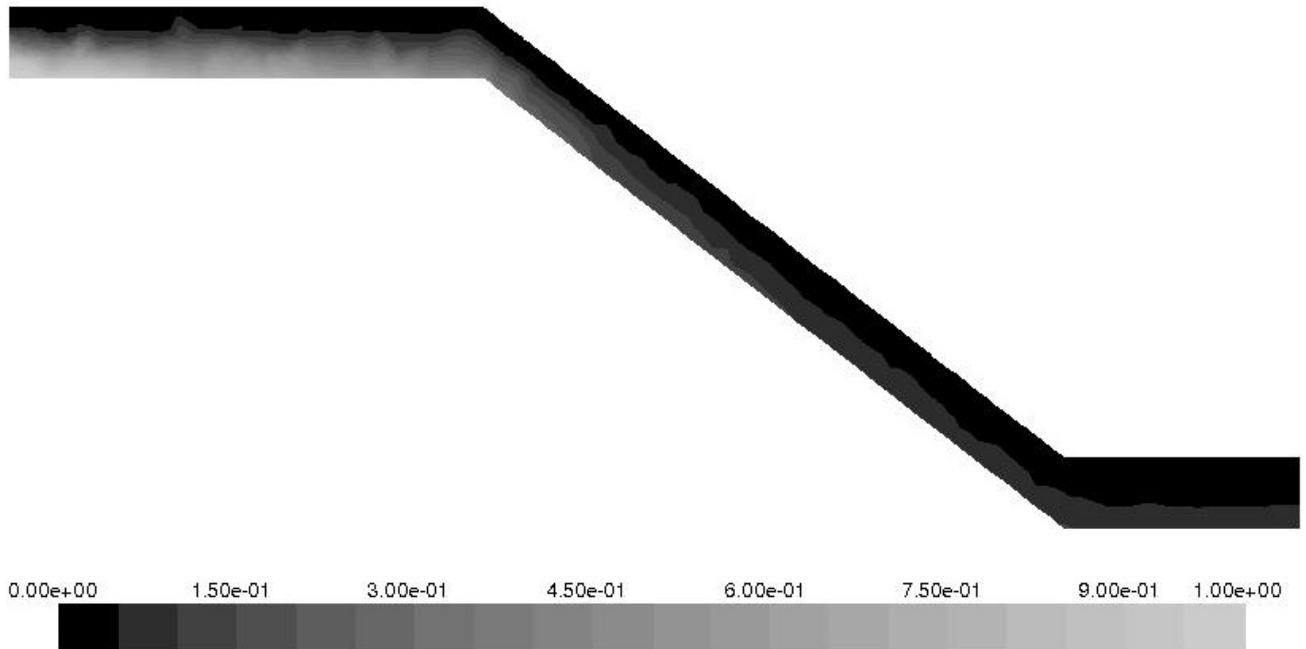


Figure 33. Contours of volume fraction of water using a very coarse tet-mesh of 4778 cells

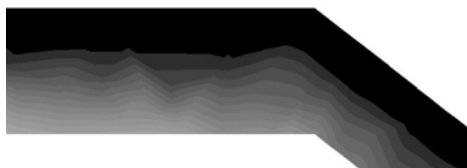


Figure 34. Zoom-up of upper part of Figure 33



Figure 35. Zoom-up of lower part of Figure 33

The next grid (see Figure 36) that was used was a fully structured one with the same equidistant interval size on all edges as the tet-mesh, 1000 mm. Since it was structured it had a lot smaller number of cells, only 732. The calculations resulted in only 0.06 kg/s difference between in- and outflow and the contours of volume fraction of water can be seen in Figure 37 - 39.

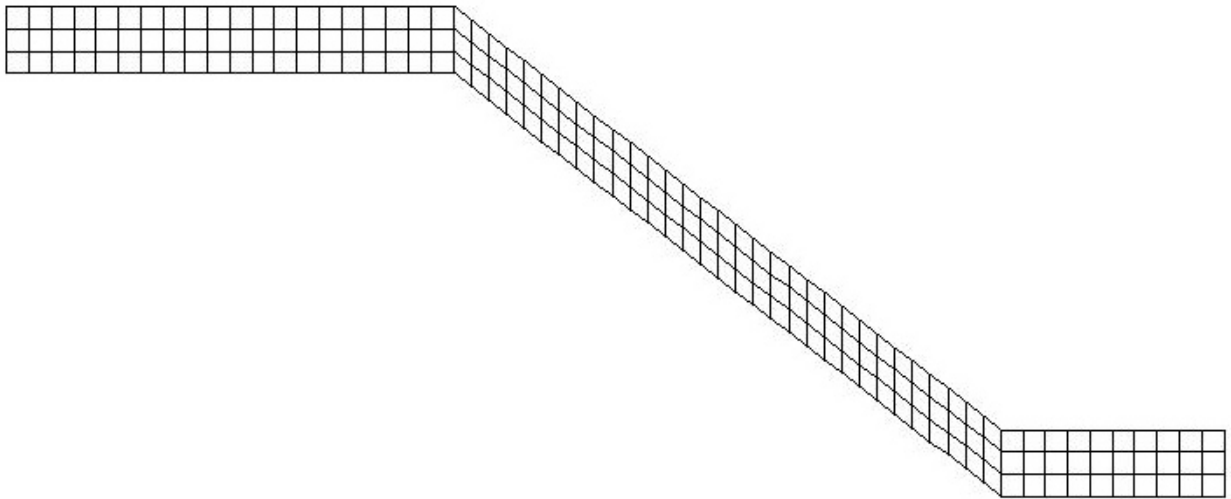


Figure 36. Cut through a hex-mesh of 732 cells

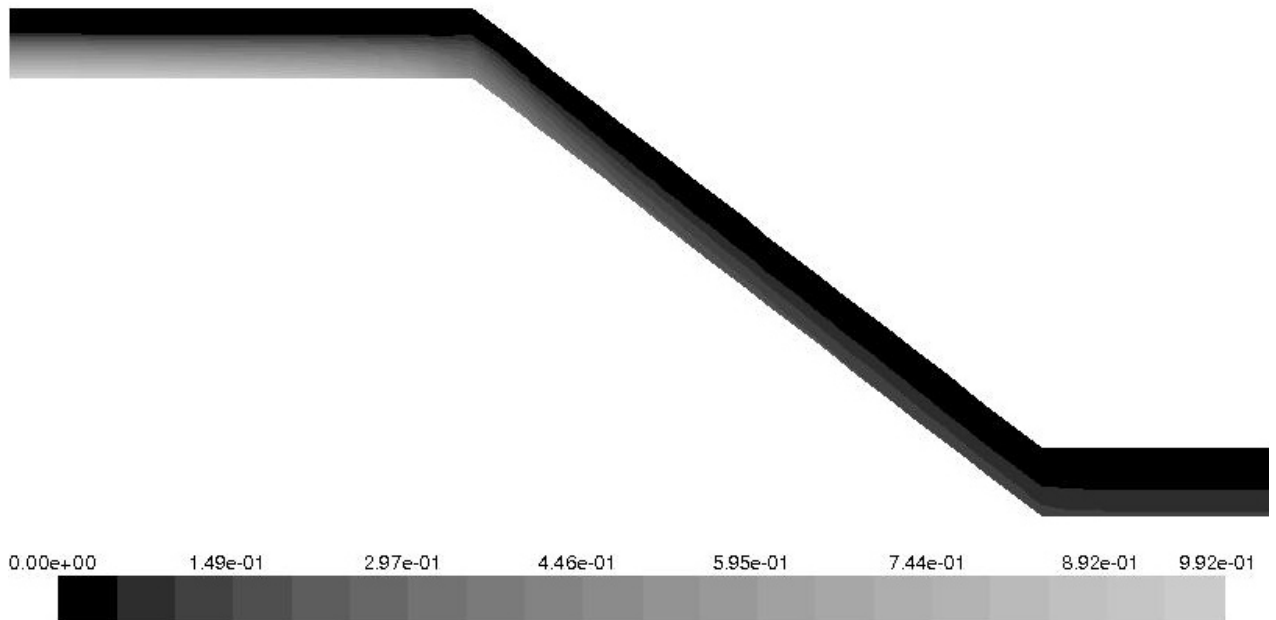


Figure 37. Contours of volume fraction of water using a very coarse hex-mesh of 732 cell

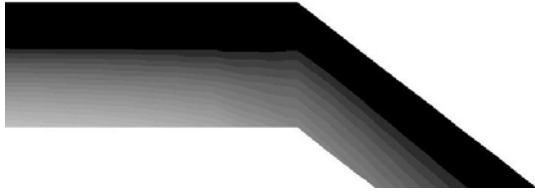


Figure 38. Zoom-up of upper part of Figure 37

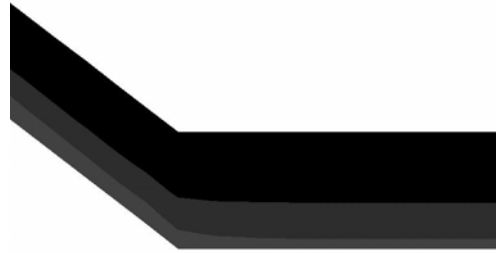


Figure 39. Zoom-up of lower part of Figure 37

These figures confirm that structured meshes are preferred rather than the unstructured ones. They are not only less expensive in terms of computational cost but also a lot more stable when using the VOF method. So the next step was to redefine the equidistant hex-mesh from the interval size of 1000 mm to 200 mm. This mesh (see Figure 40) had 91500 cells and the calculations resulted in a 0.03 kg/s difference between in- and outflow. According to Figure 41- 43 this refinement results in a considerable improvement of the surface diffusivity.

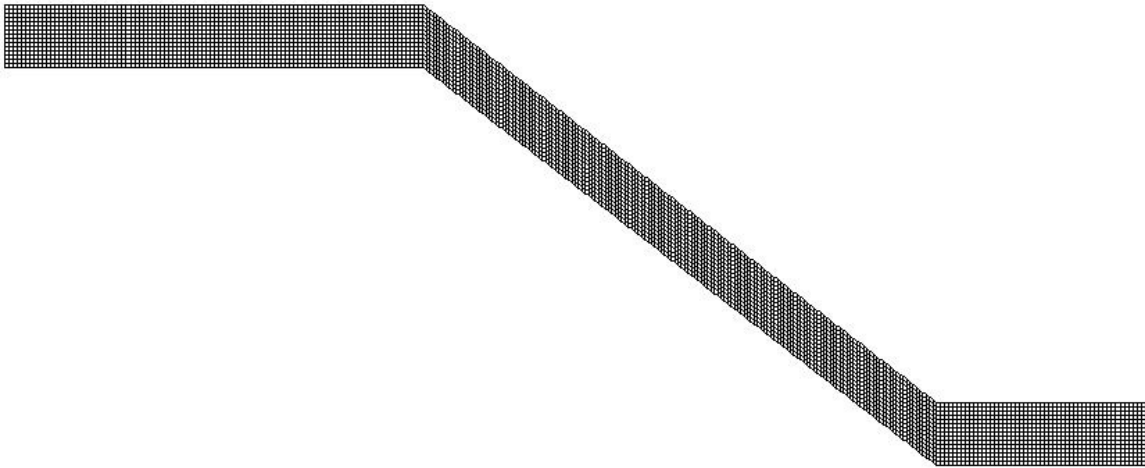


Figure 40. Cut through an equidistant hex-mesh of 91500 cells

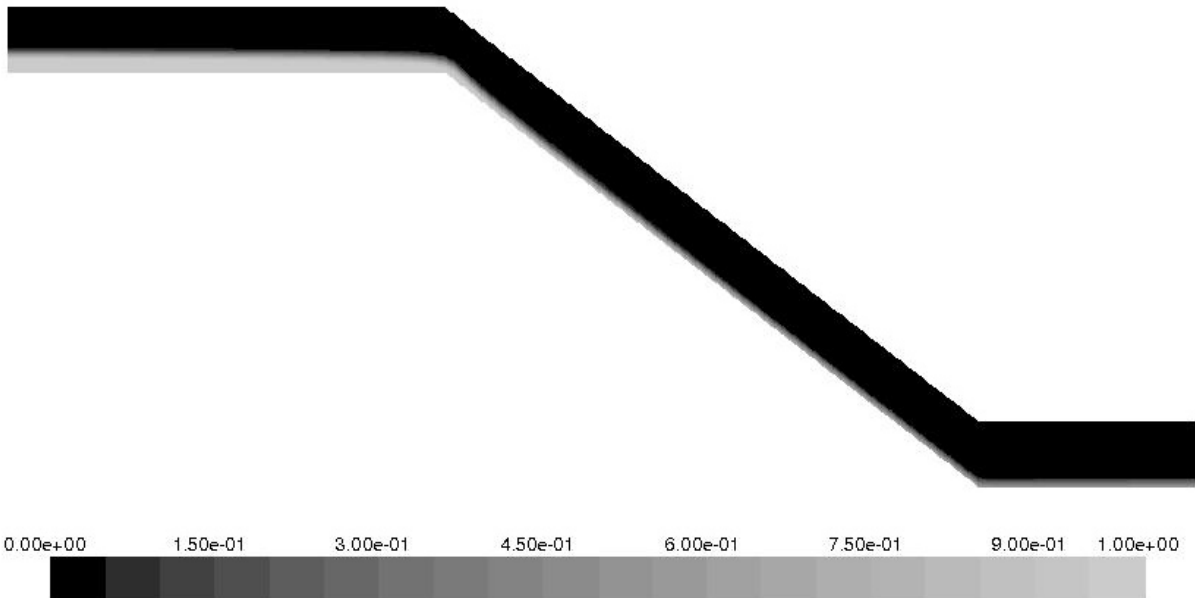


Figure 41. Contours of volume fraction of water using an equidistant hex-mesh of 91500 cells.



Figure 42. Zoom-up of upper part of Figure 41



Figure 43. Zoom-up of lower part of Figure 41

The requirement of having maximum 3 cm between the surface levels of volume fraction 0.3 and 0.7 was checked for this case by plotting the volume fraction of water as a function of the vertical distance from the bottom of the inlet (see Figure 44).

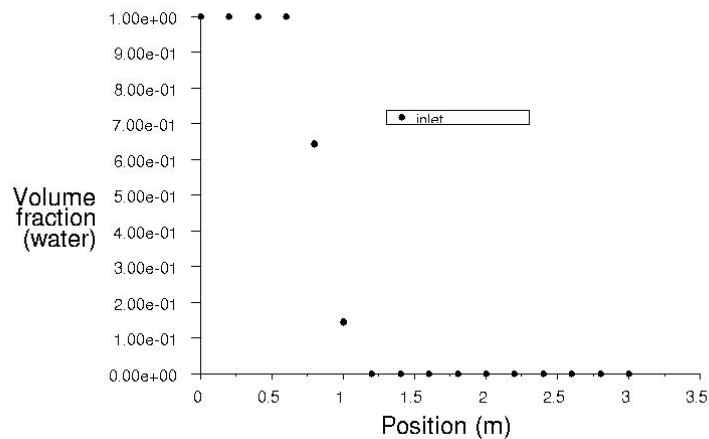


Figure 44. Volume fraction of water as function of vertical distance from the bottom of the inlet

Obviously this mesh is not fine enough for judging the level of water surface and if the 3 cm requirement is satisfied since only one value of volume fraction is between 0.3 and 0.7. Therefore some development of the mesh in the form of splitting edges and using grading was needed and done. Since the finest part of this final mesh coincides with the water surface the results for the volume fraction contours are presented without the mesh in Figure 45 - 47 and the grid itself in Figure 48.

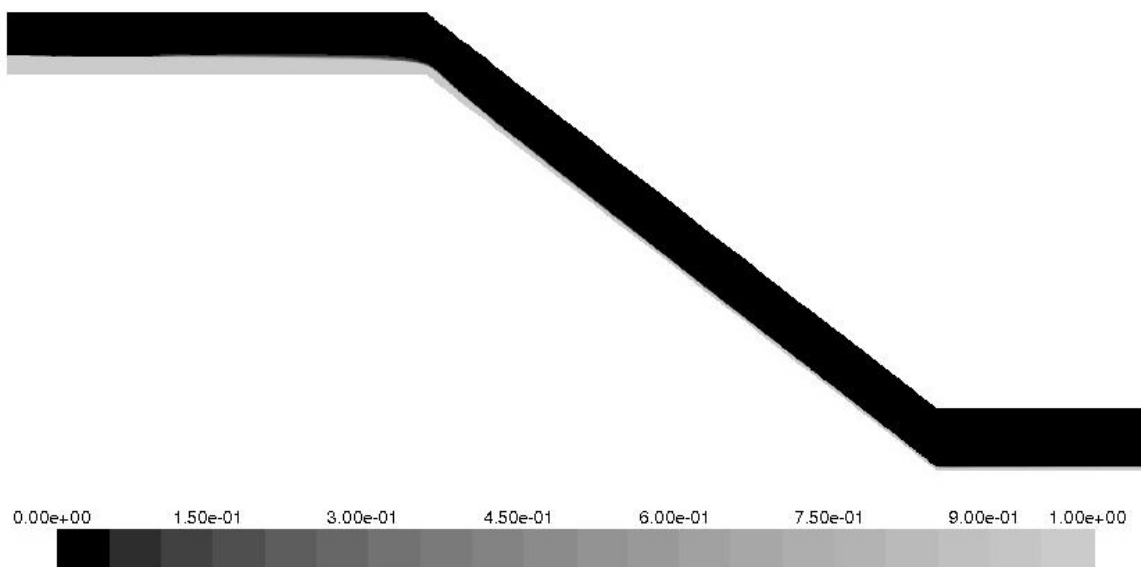


Figure 45. Contours of volume fraction of water using a refined hex-mesh of 100980 cells



Figure 46. Zoom-up of upper part of Figure 45



Figure 47. Zoom-up of lower part of Figure 45

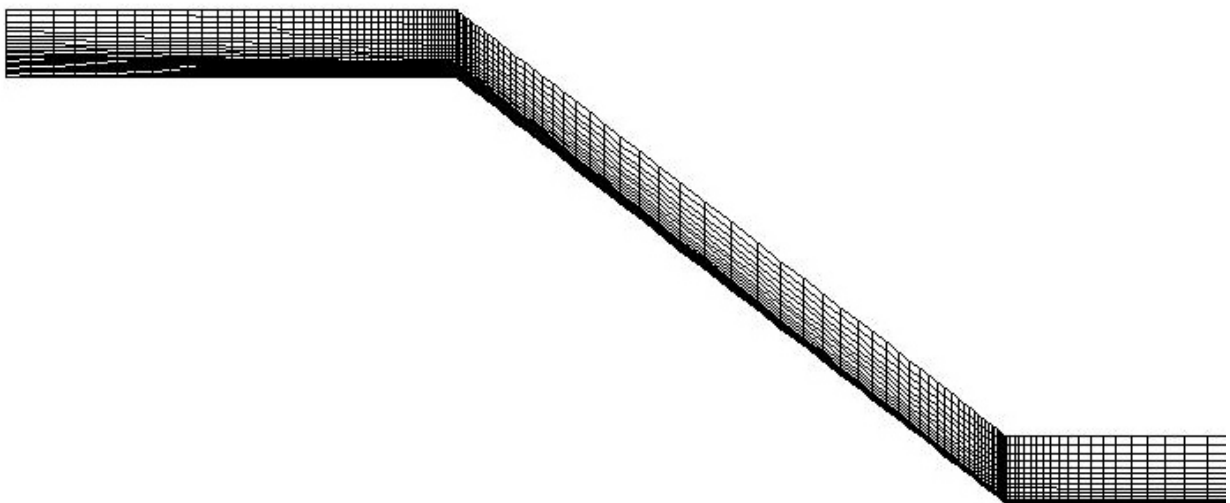


Figure 48. Cut through an unequidistant hex-mesh of 100980 cells.

Using this grid results in a very thin interface compared to the others. It was noticed that the most difficult place to determine the surface level was at the “crest” at the where the water starts its descend. When the volume fraction of water for this final case is plotted as a function of vertical distance from the crest (see Figure 49) some serious improvements in the interphase diffusivity can be witnessed.

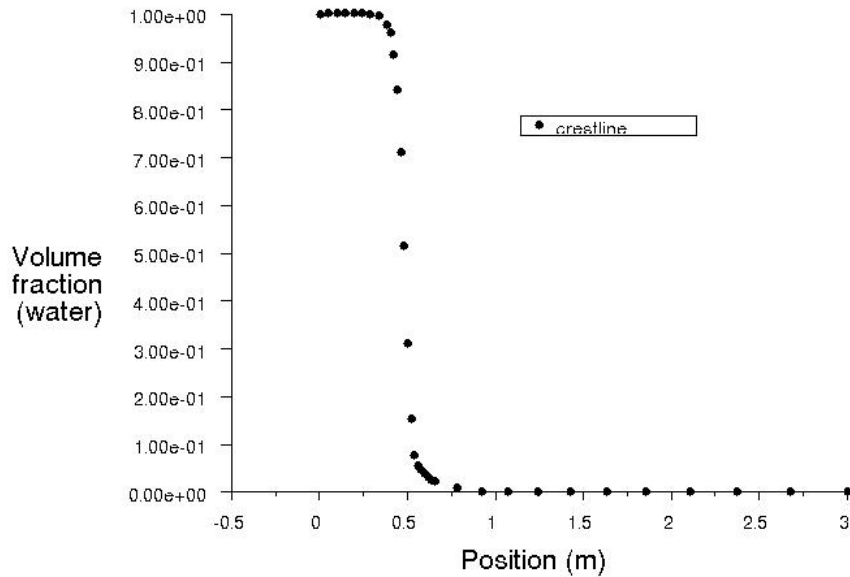


Figure 49. Volume fraction of water as function of vertical distance from the bottom of the “crest”.

The elevations of volume fractions 0.71 and 0.32 of water are 0.46 m and 0.49 m respectively so the requirement of maximum 3 cm is fulfilled. Therefore the water surface level is considered to be represented by the level of volume fraction 0.5 and in is presented in Figure 50 below with the bottom of the domain. Zoom-ups of the upper and lower parts are shown in Figures 51 – 52.

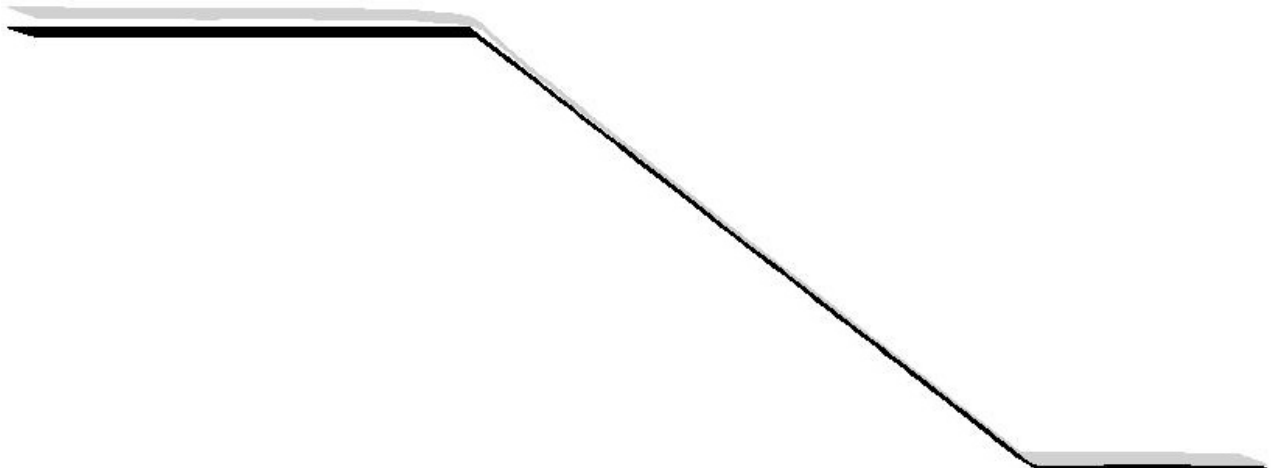


Figure 50. Isosurface with volume fraction 0.5 for water representing the water surface (grey) above the bottom of the domain.

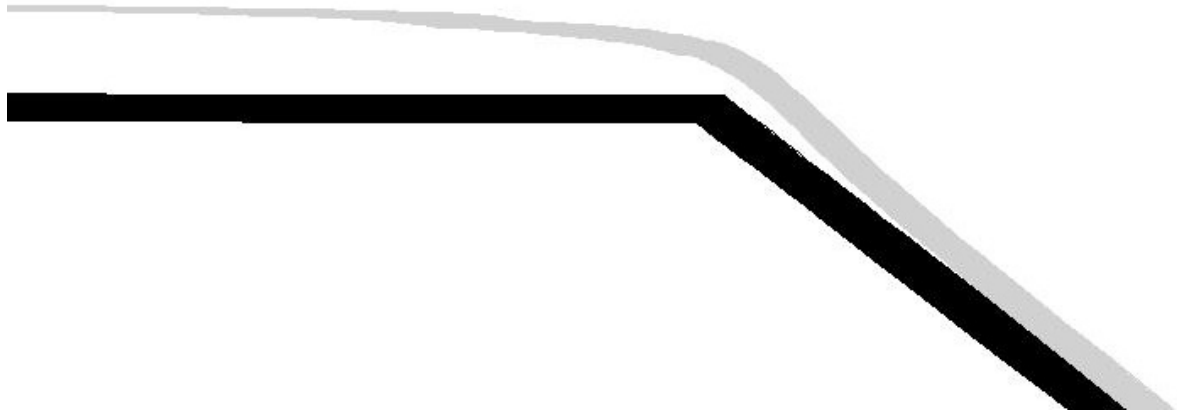


Figure 51. Zoom-up of upper part of Figure 50



Figure 52. Zoom-up of lower part of Figure 50